TAMPERE UNIVERSITY OF TECHNOLOGY

MARCOS ARIZTI

HARVESTING ENERGY FROM VEHICLE SUSPENSION

Master of Science Thesis

Supervisors: Docent Juha Miettinen
Professor Erno Keskinen

The subject has been approved in the meeting of the department council on 10.03.2010

RESUMEN

TAMPERE UNIVERSITY OF TECHNOLOGY
ARIZTI, MARCOS: Recuperación de Energía en la Suspensión de un Vehículo
Proyecto Fin de Carrera, 79 páginas, 1 Apéndice
Mayo 2010
Especialidad: Ingeniería Mecánica
Supervisores: Docente Juha Miettinen, Profesor Erno Keskinen
Palabras Clave: Recuperación de energía, suspensión, sistema hidráulico, implementación, aceleración, ser humano.

Este Proyecto Final de Carrera estudia la recuperación de energía en la suspensión de un vehículo con el objetivo de implementar un sistema eficiente sin alterar el confort del pasajero. El proyecto analiza los métodos más importantes para la recuperación de energía y selecciona los que son capaces de ser implementados en la suspensión de un vehículo. El principal logro reside en que utilizando este sistema se consigue disminuir el consumo de carburante en el vehículo.

El proyecto está dividido en tres partes. En la primera parte se exponen los métodos más relevantes para la recuperación de energía en general, enfocado desde un plano macroscópico. La segunda parte se centra en la aplicación de estos métodos para la suspensión de un vehículo, seleccionando tres entre los cuales se realiza una comparación en función de su eficiencia, resistencia, durabilidad y simplicidad. El sistema hidráulico es el que mejor cumple estos requisitos y por tanto es el que se va a simular. En la última parte correspondiente a la simulación del sistema hidráulico, se consideran cuatro modelos, empezando por un sistema sencillo de un grado de libertad y terminando con un sistema de cuatro grados de libertad que aumenta notablemente la exactitud. La simulación indica que la introducción de un sistema de recuperación de energía aumenta la aceleración vertical de un vehículo a su paso por un bache. La posibilidad de que el sistema sea perjudicial para la salud humana fija un límite que resulta ser más restrictivo que el correspondiente a la alteración del confort del pasajero. La modificación de parámetros como la velocidad y masa pueden ayudar a la reducción del valor máximo de la aceleración debida al sistema de recuperación de energía.

Los resultados de este estudio muestran que la implementación de un sistema de recuperación de energía aumenta la aceleración vertical del chasis de un vehículo, pero no necesariamente va a ser dañino para el ser humano. Finalmente, es necesario un balance entre la cantidad de energía que se puede recuperar y el confort del pasajero para determinar el coeficiente de amortiguamiento del sistema.

ABSTRACT

TAMPERE UNIVERSITY OF TECHNOLOGY
Master's Degree Programme in Mechanical Engineering
ARIZTI, MARCOS: Harvesting Energy from Vehicle Suspension
Master of Science Thesis, 79 pages, 1 Appendix pages
May 2010
Major: Mechanics and Design
Examiners: Docent Juha Miettinen, Professor Erno Keskinen
Keywords: Energy harvesting, suspension, hydraulic system, implementation, acceleration, human being.

This Master of Science thesis studies the energy harvesting in vehicle suspension. The aim of this work is to implement an efficient energy harvesting system without disturbing driver's comfort. This thesis analyzes the most relevant methods of energy harvesting and selects the ones which can be implemented in vehicle suspension. The main goal is that by using this system there is a decrease in the consumption of the fuel in the vehicle.

The thesis is divided in three sections. In the literature study section different principles of harvesting energy are explained. The most relevant ways to harvest energy are considered in this section mainly in the macro energy harvesting. In the second section three principles of implementation are considered. The selection focuses on the possibility to implementing it into the vehicle suspension. Furthermore, a comparison between them is done in terms of efficiency, resistance, reliability and simplicity is done. The hydraulic system is the most suitable one. In last section, which deals with the simulation, four models are considered, starting from the simple one with one degree of freedom, and ending with a four degree of freedom model that improve accuracy. The simulation indicates that the introduction of the energy harvesting system increases the vertical acceleration of the chassis as the vehicle passes over a bump. The human being behavior against vertical acceleration settles a restrictive limit that the vehicle has to obey. Modification in the velocity and mass could help to reduce the maximum value of the acceleration cause by the energy harvesting system.

The results of this study suggest that, by considering the hydraulic energy harvesting system the vertical acceleration in the chassis of the vehicle is going to increase but that it is not necessarily harmful for the human being. It is necessary to find the balance between the amount of energy that can be harvested and the comfortableness of the driver. This can be achieved by making use of the damping factor of the model.

PREFACE

The work of this Master of Science thesis was carried out in the Mechanics and Design Department at the Tampere University of Technology as an agreement between both Escuela Superior the Ingenieros de Bilbao and Tampere University of Technology with the assistance of the Erasmus Program.

I wish to express my sincere appreciation and gratitude to Docent Juha Miettinen for this guidance and supervision throughout this Master of Science Thesis. I am also grateful to Professor Erno Keskinen for the support and advices along the research project. I am also very grateful to Paula Cajal Mariñosa, for excellently checking English language and literature of this Master of Science thesis.

Special warm thanks to my family, my brothers Juan, Andrés and specially my parents Agustín and Natalia for their tremendous effort and continuous support during my studies and also with this Thesis work.

Last but not least, thanks to Laura, Frederico, Diego and Imanol but especially to Lucía and Enrique for their unconditional help during this year in Tampere.

Tampere, May 12, 2010

Marcos Arizti Texidó

c/Fueros 7 bajo E
48992 Bilbao, Vizcaya
Spain

TABLE OF CONTENTS

NOMENCLATURE

ζ	Damping factor
ω_n	Natural frequency
K	Stiffness
E	Modulus of elasticity
I	Moment of inertia
L	Length of a beam
b	Width of a beam
h	Thickness of a beam
P	Power generated by piezoelectric
d_{33}	Coefficient of the piezoelectric with compressive strain
d_{31}	Coefficient of the piezoelectric with transverse strain
k_{ij}	Electro mechanical coupling coefficient
W_i^e	Electrical energy stored in the i axis
W_j^m	Mechanical input energy in the j axis
k_p	Planar coupling factor
k_t	Thickness mode coupling factor
η	Efficiency of a energy harvesting system
Q	Quality factor of the generator
ε	Permittivity of the material
s	Dielectric displacement
i_p	Detectable current of a pyroelectric material
p	Pyroelectric coefficient vector
T	Temperature

C_p	Internal capacitance
C_e	External capacitor
R_e	External resistor
V_p	Element output voltage
A	Area
η_{carnot}	Carnot factor
ΔT	Temperature difference across the thermoelectric
zT	Thermoelectric figure of merit of the materials
α	Seebeck coefficient
ρ	Electrical resistivity
κ	Thermal conductivity
ZT	Average value of the components figure of merit
ΔT_{TE}	Temperature difference across thermoelectric converter
η_r	Reduced efficiency of the thermoelectric generator
k_{eff}	Thermoelectric module
V	Generated voltage
ϕ	Flux linkage
B	Magnetic flux density over the area
D_{em}	Electromagnetic damping
P_e	Electrical power in electromagnetic
R_L	Load resistance
R_c	Coil resistance
L_c	Coil inductance
d	Separation between plates in a capacitor

ε_0	Permittivity of the free space
H	Hydraulic energy in a single point
θ	Angle of the blade in a turbine
V_0	Absolute velocity value of the fluid in the entrance
$\vec{U}_2(abs)$	Absolute velocity value of the fluid in the exit
$\vec{U}_2(rel)$	Relative velocity value of the fluid in the exit
$\vec{U}_1(rel)$	Relative velocity value of the fluid in the entrance
$\vec{U}$	Velocity of the wheel
q_m	Mass flow
$\vec{P}$	Intrinsic force acting in the surface of the fluid
$\vec{G}$	Force as a result of the outside field
$\dot{\vec{M}}_2$	Amount of fluid which exit the volume
$\dot{\vec{M}}_1$	Amount of fluid which enter the volume
$\vec{R}_h$	Reaction in the fluid
$\vec{R}$	Reaction in the blade
P_{useful}	Useful power obtain by the hydraulic system
U	Fix tangential speed
r_i	Positional vectors
$\hat{n}_i$	Unit normal vectors of the surfaces
ω	Angular velocity of the wheel
P_t	Total power absorb by the fluid
ε_r	Relative permittivity of the material
v	Potential difference across the capacitor
S	Charge sensitivity

u	Coil speed
P_e	Electrical power
α_1	Angle between coil area the flux density direction
V_1	Voltage generated by electromagnetic field
Q_1	Heat converted by a thermoelectric
Q_2	Charge on both sides of the capacitor
C_2	Capacitance of the capacitor
A_2	Area of the plates in a capacitor
F_2	Perpendicular force between plates in a capacitor
A	Area in the hydraulic tube
C_1	Torque in the turbine
A_{11}	Area in the entrance of the turbine
A_{22}	Area in the exit of the turbine
U	Tangential speed for maximum power
g_1	Piezoelectric voltage constant
$[K]$	Stiffness matrix
$[C]$	Damping matrix
$[M]$	Mass matrix
$[\Omega]$	Modal matrix

1. INTRODUCTION

Energy harvesting technologies have become important in the last few years due to the amount of methods of harvesting energy and due to the different fields where they are already implemented. Powerful companies are growing, publications and articles on this topic are increasing and consequently, important advances are taking part in many industries for example in the vehicle industry. The main purpose of this study is to find all the methods of energy harvesting technologies, compare them with each other, and find the most suitable one for vehicle suspension.

The wireless sensor networks have made use of the micro energy harvesting technologies and have been introduced in many industries such as in medical, construction, air space and automotive industries among others. These sensors are usually located in places difficult to access and are powered by batteries, so it becomes hard to replace the battery once in a while. These new sensors are able to harvest enough energy to power the sensor. The sources to harvest the energy are external vibrations, radio waves, external heat or even friction. The macro energy harvesting technologies have not developed as much as the micro but in the vehicle industry the macro is becoming more important as the core competence is to save fuel. As a result of the vehicle engines have improved, the consumption has dropped and new fuels have been invented. Another way to save fuel is to recover a part of the energy which is involved in the movement of a vehicle. For this purpose they have already harvested energy from the brakes only in the F1 until now, but there are prototypes and plans to bring these advantages to the commercial vehicles.

The suspension of a vehicle is also one part of the vehicle where there is a huge amount of energy lost in friction and heat. The aim of this work is to study the different methods of harvest this energy and analyze how this would affect the passenger ergonomics. Several models are simulated with a single bump. It starts with the simplest one and single degree of freedom ending with the four degree of freedom in order to get better accuracy. The implementation of an energy harvesting system in the suspension is based on the modification of the damper making the vehicle more rigid against perturbations on the road. In addition, this modification is going to increase the vertical accelerations of the chassis that could be harmful for the human being. Furthermore, parameters such as the velocity of the vehicle and the shape of the bump are going to play an important role in the simulation part.

2. THEORICAL BACKGROUND

2.1. General Overview of energy harvesting

In the last decade, the field of energy harvesting has increasingly become important as evident from the rising number of publications and product prototypes. Several review articles have been published on this topic covering wide variety of mechanisms and techniques. The most prominent use of harvesters is to power wireless sensors node. The extreme amount of sensors that have all the devices nowadays resulted in high cost of wiring or replacing batteries (Priya, S. & Inman, D. 2009).

Energy harvesting techniques are emerging as environmental friendly energy sources, which form a promising alternative to existing energy resources. These include energy harvesting from rectennas, passive human power, wind energy and solar power (Ahmad M.E. 2005). Outdoor solar energy has the capability of providing power density of 15,000 $\mu W / cm^3$ which is about two orders of magnitude higher than other sources. However, solar energy is not attractive source of energy for indoor environments as the power density drops down to as low as 10-20 $\mu W / cm^3$. Mechanical vibrations (300 $\mu W / cm^3$) and air flow (360 $\mu W / cm^3$) are the other most attractive alternatives. In addition to this, magnetic fields that are generated by AC devices and propagate through earth, concrete, and most metals, can be source of electric energy. AC magnetic fields decrease naturally in intensity as a function of distance d from the source but also the rate of decrease can vary dramatically depending on the source (Priya, S.& Inman, D. 2009).

2.2. Different methods for energy harvesting

2.2.1. Piezoelectric

The piezoelectric effect was discovered by J. and P. Curie in 1880. They found that certain crystals were subjected to mechanical strain, they became electrically polarized and the degree of polarization was proportional to the applied strain. Piezoelectric materials are widely available in many forms including single crystals (e.g. quartz), piezoceramic (e.g. PZT), thin film and polymeric materials (e.g. PVDF). They are

widely used in numerous applications, ranging from acoustic transducers to mechanical actuators (Guillot F. M. et al. 2007).

Piezoelectric materials typically exhibit anisotropic characteristics, which mean that the properties of the material differ depending upon the direction of forces and orientation of the polarization electrodes. The piezoelectric effect converts mechanical strain into electrical current or voltage. This strain comes from many different sources. Human motion, low-frequency seismic vibrations and acoustic noise are everyday examples. Most piezoelectric electricity sources produce power in the order of milliwatts, too small for system application, but enough for hand-held devices such as some commercially-available self-winding wristwatches. The vibration of a rigid body can be caused by several factors such as unbalanced mass in a system, tear and wear of materials and occurs in almost all dynamical systems. To study the dynamic characteristics of a vibration body associated with energy harvesting is taken a single degree of freedom lumped spring mass.

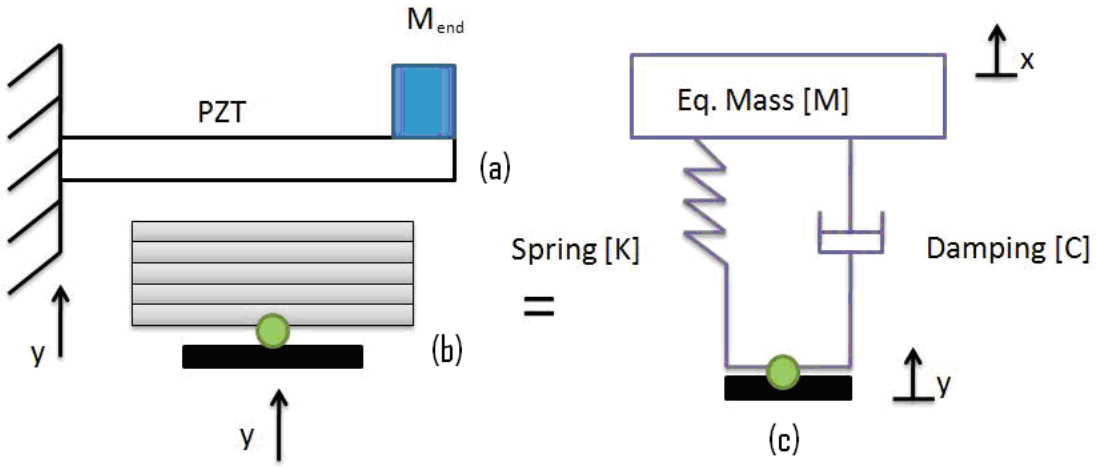

Figure 2.1. *(a) Cantilever beam with tip mass,*
(b) Multilayer PZT subjected to transverse direction,
(c) Equivalent lumped spring mass system of a vibrating rigid body.

The single degree of freedom helps to study unidirectional response of the system. Figure 2.1 shows the cantilever beam with piezoelectric plates bonded on a substrate with a proof mass at the end and multilayer piezoelectric plates. The equivalent would be the lumped spring mass with external excitation. The governing equation of motion for the system can be obtained from energy balance equation or D'Alembert's principle applies to a lumped spring mass (Priya, S. & Inman, D. 2009).

$$M\ddot{z} + C\dot{z} + Kz = -M\ddot{y} \tag{2.1}$$

where $z = x - y$ is the net displacement of mass. Equation 2.1 can also be written in terms of damping constant and natural frequency. A damping factor ς is a

dimensionless number defined as the ratio of the critical damping over the system damping.

$$\varsigma = \frac{c}{c_c} = \frac{c}{2\sqrt{mK}} \tag{2.2}$$

The natural frequency of a spring mass system is defined by the equation 2.3

$$\omega_n = \sqrt{\frac{K}{M}} \tag{2.3}$$

where the stiffness K for each loading condition should be initially calculated. For example, in case of a cantilever beam, the stiffness K is given according to

$$K = 3EI / L^3 \tag{2.4}$$

where E is the modulus of elasticity, I is the moment of inertia, and L is the length of beam. The moment of inertia for a rectangular cross-sectional can be obtained from the expression

$$I = (1/12)bh^3 \tag{2.5}$$

where b and h are the width and thickness of the beam in transverse direction, respectively. The power output of piezoelectric system will be higher if system is operating at natural frequency. The natural frequency dictates the selection of materials and dimensions and it is important not be confused with natural frequency of mechanical system.

The ratio of output $z(t)$ and input $y(t)$ can be obtained by applying Laplace transform with zero initial condition.

$$\left|\frac{Z(s)}{Y(s)}\right| = \frac{s^2}{s^2 + 2\varsigma\omega_n + \omega_n^2} \tag{2.6}$$

By applying the inverse Laplace transform on equation 2.1 and assuming that the external base excitation y is sinusoidal.

$$y = Y\sin(\omega t) \tag{2.7}$$

is possible to obtain the time domain response.

$$z(t) = \frac{\left(\frac{\omega}{\omega_n}\right)^2}{\sqrt{\left(1-\left(\frac{\omega}{\omega_n}\right)^2\right)^2 + \left(2\varsigma\frac{\omega}{\omega_n}\right)^2}} Y\sin(\omega t - \phi) \tag{2.8}$$

The approximate mechanical power of a piezoelectric transducer vibrating is obtained from the product of velocity and force of the mass as

$$P(t) = \frac{m\varsigma Y^2\left(\frac{\omega}{\omega_n}\right)^3 \omega^3}{\left(1-\left(\frac{\omega}{\omega_n}\right)^2\right)^2 + \left(2\varsigma\frac{\omega}{\omega_n}\right)^2} \tag{2.9}$$

The maximum power is calculated by setting the operating frequency as natural frequency:

$$P_{\max} = \frac{mY^2\omega_n^3}{4\varsigma} \tag{2.10}$$

Power can be maximized by lowering damping, increasing natural frequency, mass and amplitude of excitation.

The common methods utilized for piezoelectric energy harvesting are 33-mode (stack actuators) and 31-mode (bimorphs). In the 33-mode the direction of applied stress force and generated voltages is the same, while in 31-mode the stress is applied in the axial direction but the voltage is obtained from the perpendicular direction. In the case of a multimorph structure, when the structure resonates, an alternating voltage is produced as a consequence of piezoelectric d_{31} effect. Thus, the forces induced on the upper piezoelectric element generate a voltage of the same polarity as the poling voltage (Swee, L. Kok et al. 2009).

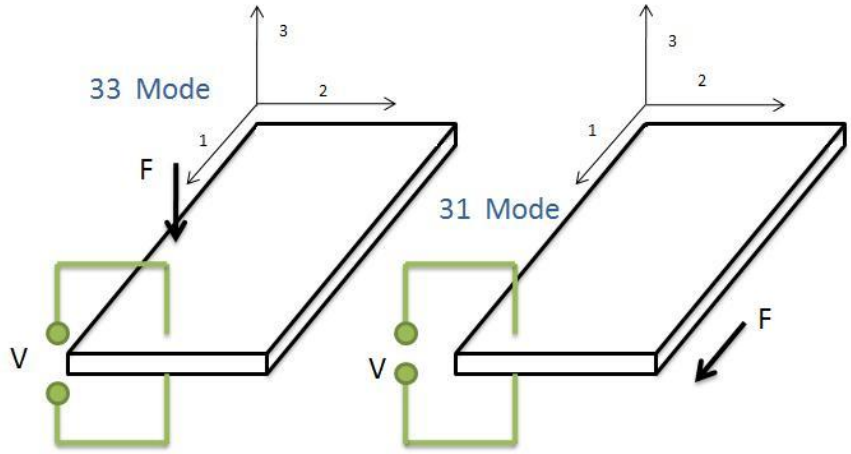

Figure 2.2. *Operating modes of piezoelectric transducers.*

In the real case there will be a continuous system that has an infinite number of natural frequencies and that is why the lumped spring mass system may not provide a reasonable estimate of the output.

The level of piezoelectric activity of a material is defined by series of constant used in conjunction with the axes notation. The piezoelectric strain constant d can be defined as

$$d = \frac{strain\_developed}{applied\_field} m/V$$

$$d = \frac{short\_circuit\_charge\_density}{applied\_stress} C/N$$

The piezoelectric generators which operate with a compressive strain (33-mode) exploit the d_{33} coefficient of the material while the one with transverse strain (31-mode) exploit the d_{31} coefficient. The power output achieved in the compressive mode can be improved by increasing the piezoelectric element's thickness or by using a multi-layer stacks.

Another important constant affecting the generation of the electrical power is the electro-mechanical coupling coefficient *k*, it describes the efficiency with which the energy is converted by the material between electrical and mechanical forms in a given direction and is represented by the equation 2.11.

$$k_{ij}^2 = \frac{W_i^e}{W_j^m} \tag{2.11}$$

where W_i^e, is the electrical energy stored in the i axis and W_j^m is the mechanical input energy in the j axis. Moreover, k_p is defined as the planar coupling factor which is used for radial modes of thin discs and k_t is defined as the thickness mode coupling factor for a plate or disk.

The efficiency of energy conversion, η, for a piezoelectric element clamped to a substrate and cyclically compressed at its resonant frequency is given by

$$\eta = \frac{\dfrac{k^2}{2(1-k^2)}}{\dfrac{1}{Q} + \dfrac{k^2}{2(1-k^2)}} \tag{2.12}$$

where Q is the quality factor of the generator.

In addition to these there are other relevant constants such as the permittivity of the material, ε, and dielectric displacement per unit electric field and compliance, s, which is the strain produced per unit of stress. Lastly, the piezoelectric voltage constant, g_1, is defined as the electric field generated per unit of mechanical stress (Priya, S. & Inman, D. 2009).

The piezoelectric properties vary with age, stress and temperature. The change in the properties of the piezoceramic with time is known as the ageing rate and is dependant on the construction methods and the material type. The ageing process is accelerated by the amount of stress applied to the ceramic and this should be considered in cyclically loaded energy harvesting applications. One proposal is that they are used for micro-scale devices, such as in a device harvesting micro-hydraulic energy. In this device, the flow of pressurized hydraulic fluid drives a reciprocating piston supported by three piezoelectric elements which convert the pressure fluctuations into an alternating current.

Piezoelectric systems can convert motion from the human body into electrical power. It is possible to harvest energy from leg and arm motion, shoe impacts and blood pressure for low level power to implantable or wearable sensors. Also the piezo can be integrated into clothing with careful design to minimize user discomfort. Furthermore, piezoelectric elements are being embedded in walkways to recover the “people energy” of footsteps and even embedded in shoes to recover “walking energy”.

2.2.2. Pyroelectric

The pyroelectric effect converts a temperature change into electrical current or voltage and it is analogue to the piezoelectric effect, which is another type of ferroelectric behavior. Like piezoelectricity, pyroelectricity requires time-varing inputs and suffers from small power outputs in energy harvesting applications.

One key advantage of pyroelectrics over thermoelectrics is that many pyroelectric materials are stable up to 1200 degrees or more, enabling energy harvesting from high temperature sources and thus increasing thermodynamic efficiency. The energy-harvesting device uses the edge-depolarizing electric field of a heated pyroelectric to convert heat energy into mechanical energy instead of drawing electric current off two plates attached to the crystal-faces.

Several factors must be considered to optimize the performance of such materials for a given application, such as the material's geometry, boundary conditions, and even the circuitry used to harvest power must be carefully considered. In terms of geometry high thermal mass may increase the time it takes to heat and cool the material.

One possibility to improve energy generation is to use pyroelectric materials with significantly higher pyroelectric coefficients. A recent study showed that thin films with volume fractions similar to bulk PZT exhibit orders of magnitude higher pyroelectric coefficients. The use of pre-stressed materials may also enhance performance.

In order to understand the operating principle and to exhibit the pyroelectric effect is considered a material's temperature change with respect to time (temporal fluctuation) that results in the production of electric charge. In particular, the detectable current $i_p(t)$ of a pyroelectric material is proportional to the rate change of its temperature.

$$i_p(t) = p' \; A\frac{dT(t)}{dt} \tag{2.13}$$

where p' is the component of the pyroelectric coefficient vector p orthogonal to the electrode surface of area A; and $T(t)$ denotes the temperature with respect to time. The heating and the cooling behavior of the material is not considered in the model.

The pyroelectric element is modeled as a current source $i_p(t)$ in parallel with an internal capacitance C_p. The Figure 2.3 shows the pyroelectric element connected in parallel with an external capacitor C_e and the resistor R_e. The objective is to determine the element's output voltage $V_p(t)$ and the power $P(t)$ generated for a given temperature profile $T(t)$.

For a given temperature profile $T(t)$, the instantaneous power dissipated by the resistor R_e can be determined by measuring the output voltage $V_p(t)$

$$P(t) = \frac{V_p^2(t)}{R_e} \tag{2.14}$$

On the other hand, the generated power can be predicted using (2.10) and assuming zero initial conditions. After this, summing currents in the circuit shown in the Figure 2.3

$$p'AsT(s) = CsV_p(s) + \frac{1}{R_e}V_p(s) \tag{2.15}$$

where s is the Laplace variable and $T(s)$ and $V_p(s)$ are the Laplace transforms of the temperature and output voltage, respectively. Therefore, the transfer function relating the input temperature $T(s)$ to the output voltage $V_p(s)$ is:

$$G(s) \cong \frac{V_p(s)}{T(s)} = \frac{p'As}{Cs + 1/R_e} \tag{2.16}$$

Finally, the predicted power generation based on a given temperature profile $T(t)$ for the pyroelectric element can be determined first by using (2.13) to determine the output voltage $V_p(t)$. Then, the power across the resistor can be calculated using (2.11). The thermal dynamic effects such as the heating and cooling rate of the pyroelectric element are not considered in the above expression.

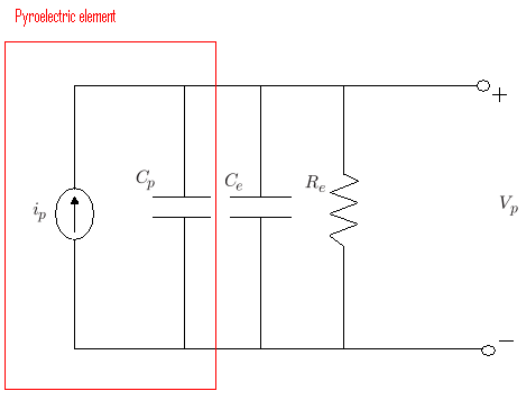

Figure 2.3. *A lumped-parameter model of a pyroelectric element, which is modeled as a current $i_p(t)$ in parallel with an internal capacitance C_p, connected in parallel to an external capacitor C_e and resistor R_e. The current i_p is proportional to the rate of change of temperature of the device. The voltage generated by the pyroelectric element is denoted by $V_p(t)$.*

2.2.3. Thermoelectric

In 1821 Thomas Johann Seebeck discovered that a thermal gradient formed between two dissimilar conductors produces a voltage. The fact is that a temperature gradient in a conducting material results in heat flow and in the diffusion of charge carriers. The flow of charge carriers between the hot and cold regions in turn creates a voltage difference. In 1834 Jean Charles Athanase Peltier discovered that running an electric current through the junction of two dissimilar conductors could, depending on the direction of current flow, cause it to act as a heater or cooler. The heat absorbed or produced is proportional to the current and the proportionality constant is known as the Peltier coefficient. Today, due knowledge of the Seebeck and Peltier effects thermoelectric materials can be used as heaters, coolers and generators.

Ideal thermoelectric materials have a high Seebeck coefficient, high electrical conductivity and low thermal conductivity. Low thermal conductivity is necessary to maintain a high thermal gradient at the junction. The most important advantage of the thermoelectrics is that no moving parts allow continuous operation for many years, as they contain no materials that must be replenished. One downside to thermoelectric energy conversion is low efficiency (currently less than 10%). The development of materials that are able to operate in higher temperature gradients and that can conduct electricity well without conducting heat at the same time will result in increased efficiency.

Another disadvantages is that the useful work content of heat is limited by Carnot factor

$$\eta_{Carnot} = \frac{\Delta T}{T_h} \tag{2.17}$$

where $\Delta T = T_h - T_c$ is the temperature difference across the thermoelectric. This puts thermoelectric energy harvesting at a distinct disadvantage when compared with the other forms of energy harvesting that are not Carnot limited.

Standard thermoelectric modules manufactured today consist of P- and N-doped bismuth-telluride semiconductors sandwiched between two metallized ceramic plates. The ceramic plates add rigidity and electrical insulation to the system. The semiconductors are connected electrically in series and thermally in parallel.

A thermoelectric generator utilizes heat flow across a temperature gradient to power an electric load through the external circuit. The temperature difference provides the voltage ($V = \alpha \Delta T$) from the Seebeck effect, while the heat flow drives the electrical current. The combination of voltage and electrical current determines the power output.

The thermoelectric *figure of merit* of the materials (zT) depends on the Seebeck coefficient (α), absolute temperature (T), electrical resistivity (ρ), and thermal conductivity (κ) of the material:

$$zT = \frac{\alpha^2 T}{\rho\kappa} \tag{2.18}$$

The maximum efficiency of a thermoelectric device is determined by its figure of merit (ZT), which is largely an average of the component materials zT values. Concerning the efficiency a thermoelectric generator converts heat Q into electrical power P_e with efficiency η

$$P_e = \eta Q \tag{2.19}$$

The maximum efficiency of a thermoelectric converter depends heavily on the temperature difference ΔT_{TE} across the device. This is because the thermoelectric generator, like all heat engines, cannot have an efficiency greater than Carnot cycle

$$\eta = \Delta T_{TE} \frac{\eta_r}{T_h} \tag{2.20}$$

where η_r is the reduced efficiency, the efficiency relative to the Carnot efficiency.

The efficiency of a thermoelectric generator increases nearly linearity with temperature difference indicating η_r / T_h is fairly constant. In energy harvesting applications, where the temperature difference ΔT is small, the efficiency is approximately directly proportional to the ΔT across the thermoelectric.

It is also important to take into account that obviously as bigger as the device is it utilizes more heat Q and will produce more power P. Similarly the use of twice power converters will naturally produce twice the power and consume twice the heat. According to that it is better to focus on power per unit harvested area (P/A) produced and heat flux (Q/A) rather than absolute power and heat consumed. This is interesting in thermoelectric power generation due to the advantage that a large system can simply be an array of smaller systems

$$\frac{P}{A} = \eta \frac{Q}{A} \tag{2.21}$$

This means that for a maximum power flux (P/A), it is necessary to maximize both heat flux (Q/A) and efficiency.

At a constant temperature difference across the thermoelectric (ΔT_{TE}) and the thermal conductance ($K = \kappa A / l$), the inverse of thermal resistance and therefore, the heat/area absorbed into the thermoelectric generator, can be modified by adjusting its height, *l*, resulting in,

$$\frac{Q}{A} = \frac{\kappa_{eff} \Delta T_{TE}}{l} \tag{2.22}$$

The effective thermal conductivity, κ_{eff}, of the thermoelectric module depends not only on the thermal conductivity of the n- and p-type materials but also on the thermoelectric materials filling fraction, parallel heat losses within the module, and Peltier effect.

In the last few years recently developed thin films devices have very slight thermoelectric material, ranging about 0.0005 to 0.004cm. In out-of-plane devices this provides a very small value for l, which allows exceptionally high-heat fluxes and low-thermal resistances. These films have the greatest advantage when the heat exchanges are nearly ideal, having very low-thermal resistances, such as in forced water cooling. On the other hand these devices have lower efficiency due to the larger fraction of electrical and thermal contact resistance losses.

Thin film thermoelectrics used in the in-plane direction have the capability of producing a much greater number of higher thermal impedance couples. Larger number of couples produces significantly higher voltage and higher thermal impedance is more appropriate for low-heat flux energy-harvesting applications. The inherent disadvantage of in-plane thermoelectrics is that the substrate used to deposit the thermoelectrics acts as a thermal short, reducing the efficiency (Priya, S. & Inman, D. 2009).

Miniature thermocouples have been developed that convert body heat into electricity and generate 40uW at 3V with a 5 degree temperature gradient, while thermocouples are used in nuclear RTG batteries.

2.2.4. Ambient radiation sources (RF)

A possible source of energy comes from ubiquitous radio transmitters. Unfortunately, is necessary a large collection area or close proximity to the radiating source to get useful power levels from this source. RF energy harvesting converts radio waves into DC power. This is accomplished by receiving radio waves with an antenna, converting the signal and conditioning the output power.

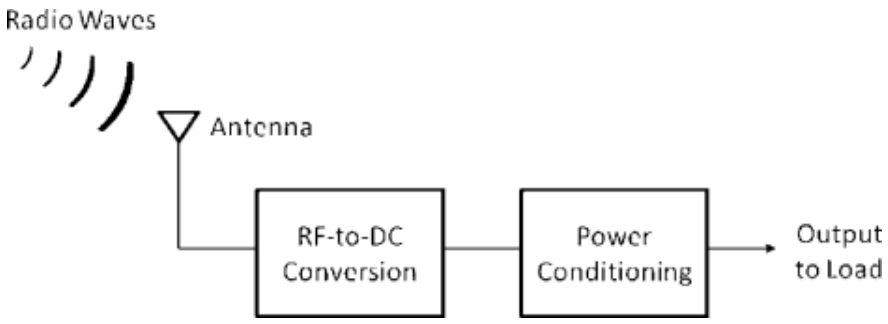

Figure 2.4. *Overview of an RF energy harvesting.*

There are multiple approaches to convert an RF signal to DC power depending on the desired operating parameter, such as power, efficiency or voltage. The amount of power available for the end device depends on several factors including the source power, distance from the source, antenna gain and conversion efficiency.

The sources for energy harvesting can be divided into three general categories: (1) intentional sources, which are the ones that provide the most control because the availability and amount of power can be controlled and engineered for the application, (2) anticipated ambient sources, like radio television etc... that although there is no control they can be relied on to act as sources, of power on a regular or intermittent basis, and finally (3) the unknown ambient sources which are the sources of RF energy where there is no control and no knowledge but which still provide a continual or intermittent source of power.

Comparisons are often made regarding the power density but it is also incomplete because each type of energy harvesting presents unique benefits. In the case of RF energy harvesting is: controllable, ambient power over distance, one to many wireless power distribution, mobility and independence of weather conditions or time day.

RF energy harvesters can be simplex or complex depending on the performance and functionality required. A simplex harvester may provide basics signal rectification and require external power management's circuitry and a complex harvester may combine the power management and other functionality within a single component.

The important characteristics is that a commercial RF energy harvester should provide are: flexibility, application flexibility, high sensitivity to enable it to harvest from ultralow levels of RF energy and high efficiency to convert as much of that energy as possible into usable power. Furthermore, it is important that the efficiency range should be sufficient broad to support a wide range of operating conditions such as input power, load resistance and output voltage. Lastly, there are becoming important the intelligent power management capabilities, which can be controlled or used by a microcontroller to optimize system-level power.

There are multiple ways to use RF energy harvesting in implementing a power system like: direct power (no energy storage), battery-free energy storage (supercapacitor), battery-recharching, remote power with battery backup and passive wireless switch (battery activation). These implementation options provide significant flexibility in designing power systems for wireless sensors

The applications include ground level agricultural sensors, structural health monitoring, distributed pollution sensors and rotational equipment sensors. RF energy harvesting has great potential to power systems for indoor usage such as temperature, motion and light sensors. Ambient RF power levels will increase as more transmitting devices are put into use.

The development of efficient multiband or wideband RF energy harvesters will also play an important role in the realization of widespread ambient harvesting over the next several years. RF energy harvesting is a unique technology that can enable controllable, wireless power over distance and scale to provide power to thousands of wireless

sensors. Devices built with this technology can be sealed, embedded within structures or made mobile and battery replacement can be eliminated. Engineers can integrate this technology to provide embedded wireless devices (Ostaffe, H. 2009).

2.2.5. Electromagnetic

Electro-magnetism has been used to generate electricity since the early 1930s, not long after Faraday's fundamental breakthrough in electromagnetic induction. The majority of the generators used today is based on rotation and are used in numerous applications from the large-scale generation of power to smaller scale applications in cars to recharge the battery.

The basic principle is based on Faraday's law of electromagnetic induction. In 1831, Michael Faraday discovered that when an electric conductor is moved through a magnetic field, a potential difference is induced between the ends of the conductor. The electromotive force (e.m.f.), induced in a circuit is proportional to the time rate of change of the magnetic flux linkage of that circuit

$$V_1 = -\frac{d\phi}{dt} \tag{2.23}$$

where V_1 is the generated voltage or induced e.m.f and ϕ is the flux linkage. In most of the applications the circuit consist of a coil of wire with multiples turns and the magnet field is created with permanent magnets, so the voltage induced is given by

$$V_1 = -N\frac{d\phi}{dt} \tag{2.24}$$

In general flux linkage for a multiple turn coil should be evaluated as the sum of the linkages for the individual turns

$$\phi = \sum_{i=1}^{N} \int_{A_i} B \cdot dA \tag{2.25}$$

where B is the magnetic flux density over the area of the i th turn. In the case where the flux density can be considered uniform over the area of the coil, the integral can be reduced to the product of the coil area, number of turns and the component of flux density normal to the coil area

$$\Phi = NBA\sin(\alpha_1) \tag{2.26}$$

where α_1 is the angle between the coil area and the flux density direction. According to this the induced voltage can be calculated

$$V_1 = -NA\frac{dB}{dt}\sin(\alpha_1) \tag{2.27}$$

In most linear vibration generators, the motion between the coil and the magnet is in a single direction for example x-direction and the magnetic field B is produced by the permanent magnet and has no time variations, so in this case the voltage equation simplifies

$$V_1 = -\frac{d\Phi}{dx}\frac{dx}{dt} = -N\frac{d\phi}{dx}\frac{dx}{dt} \tag{2.28}$$

To extract power from generator the coil terminals must be connected to a load resistance R_L allowing a current to flow in the coil. The interaction between the field caused by the induced current and the field from the magnets gives rise to a force which opposes the motion and is proportional to the current and the velocity

$$F_{em} = D_{em}\frac{dx}{dt} \tag{2.29}$$

Maximizing the power in the form of electrical energy involves the maximization of the electromagnetic damping D_{em}. As a result of this is important to know which parameters can be used to maximize electromagnetic damping. The instantaneous power extracted is shown in the equation below

$$P_e = F_{em}(t)dx(t)/dt \tag{2.30}$$

And this power is dissipated in the coil and load impedance

$$F_{em}\frac{dx}{dt} = \frac{V_1^{\,2}}{R_L + R_C + jwL_C} \tag{2.31}$$

where R_L, R_C are the load and coil resistances respectively and L_C the coil inductance. Taking equation (2.23) and (2.24) and substituting in (2.26) the result is an expression for the electromagnetic damping

$$D_{em}\left(\frac{dx}{dt}\right)^2 = \frac{\left(\frac{d\phi}{dx}\right)^2 \cdot \left(\frac{dx}{dt}\right)^2}{R_L + R_C + jwL_C} \tag{2.32}$$

Simplifying the equation (2.27) we got

$$D_{em} = \frac{1}{R_L + R_C + jwL_c}\left(\frac{d\Phi}{dx}\right)^2 \tag{2.33}$$

The idea will be to maximize the flux linkage gradient and minimizing the coil impedance (Priya, S. & Inman, D. 2009).

2.2.6. Electrostatic

This type of harvesting is based on the changing capacitance of vibration-dependent varactors (varactors are principally used as a voltage-controlled capacitor). Vibrations separate the plates of an initially charged varactor (variable capacitor) and mechanical energy is converted into electrical energy.

To harvest mechanical vibration is necessary to create an artificial mechanical reference to translate the relative displacement between the vibration source and this inertial mass in electrical energy by a mechanical to electrical converter. The main limitation is that the input vibration is given by the environment and can not be change, in order to minimize the system size a optimization of the inertial mass is needed.

Regarding the operation principle a capacitor consists of two plates which are electrically isolated each other typically by air, vacuum or an insulator. The charging of the plates by a battery of voltage V_2 creates equal but opposite charges on the plates Q_2 leading to storage of the charge when the voltage source is disconnected.

The fundamental definition of the capacitance of such a capacitor is

$$C_2 = \frac{Q_2}{V_2} \tag{2.34}$$

where C_2 is the capacitance in farads, Q_2 is the charge on the plate in coulombs and V_2 is the voltage on the plates in volts. For a parallel plate capacitor, the capacitance is

$$C_2 = \varepsilon \frac{A_2}{d} \tag{2.35}$$

where, ε is the permittivity in farads of the material between the plates in Fm^{-1}. A_2 is the area of the plates in m^2 and d is the separation between the plates in m.
If ε_0 is the permittivity of the free space equation 2.35 can be expressed in terms of the dielectric constant, $\kappa = \varepsilon / \varepsilon_0$ of the insulator material

$$C_2 = \kappa\varepsilon_0 \frac{A_2}{d} \tag{2.36}$$

The voltage across a parallel plate capacitor involves the capacitance, distance, permittivity and area

$$V_2 = \frac{Q_2 \cdot d}{\varepsilon_0 \cdot A_2} \tag{2.37}$$

The energy stored in a capacitor, with plate charge Q_2 and potential difference V_2, is given by

$$E = 0.5Q_2V_2 = 0.5C_2V_2^{\ 2} = 0.5\frac{Q_2^{\ 2}}{C_2} \tag{2.38}$$

If the charge on the plates is held constant the perpendicular force between the plates is shown in the equation below

$$F_2 = 0.5Q_2 \frac{2d}{\varepsilon A_2} \tag{2.39}$$

If the voltage between the plates is held constant the perpendicular force between the plates is given by:

$$F_2 = 0.5\frac{\varepsilon A_2 V_2^{\ 2}}{d^2} \tag{2.40}$$

The work done against the electrostatic force between the plates provides the harvested energy.

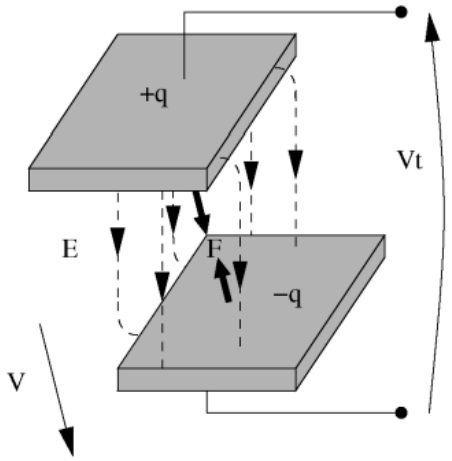

Figure 2.5. *Electrostatic transducer adapted from (Mitcheson & Yeatman, 2009).*

Electrostatic generators can be classified into three types:

1.-In plane overlap varying
2.-In plane gap closing
3.-Out of plane gap closing
(Beeby, S.P. 2006)

2.2.7. Hydraulic

The hydraulic harvest technologies have not been developed until few years ago when students from the MIT created Levant Corporation as a consequence of the idea to harvest energy from the suspension of a vehicle. This was based in the hydraulic principle.

The external forces actuating in the piston pressurize the fluid inside it, and with a hydraulic turbine the pressure is converted into a rotation in a shaft. Finally, with an electric generator is possible to obtain electricity. The fluid compressed inside the piston must go through external tubes, decreasing its pressure but increasing the speed as Bernoulli shows

$$H = \frac{P}{\gamma} + z + \frac{v^2}{2 \cdot g} \tag{2.41}$$

Using Bernoulli between two different points (1) in the piston and the other (2) in the external tube and depreciating the variation of height between the two points ($z_1 \cong z_2$) is possible to see the first deduction (see Figure 2.6). It is important to take into account that volume of flow will remain constant ($Q = v \cdot A$, where A is the area)

$$\frac{P_1}{\gamma} + z_1 + \frac{v_1^2}{2g} = \frac{P_2}{\gamma} + z_2 + \frac{v_2^2}{2g} \tag{2.42}$$

where $\gamma = \rho \cdot g$ and ρ is the density and g the gravity, P is the pressure z the height and v the speed.

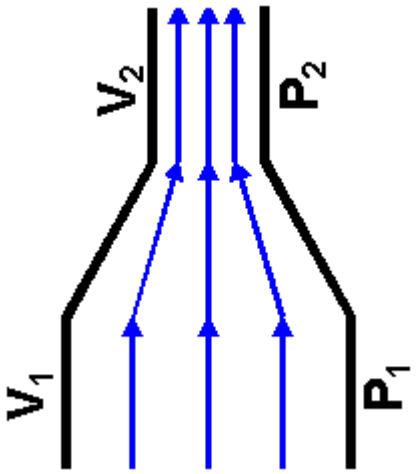

Figure 2.6. *Exit of the piston and beginning of the tube.*

Using sensors of pressure it will be possible to calculate the difference of pressure between both sections.

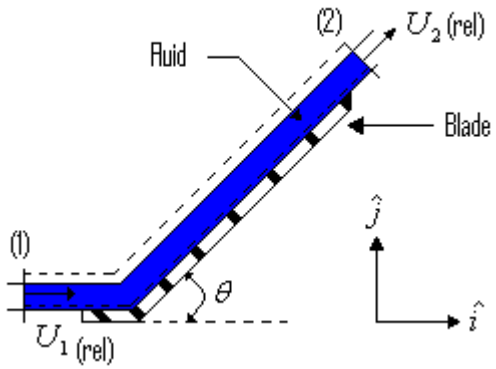

Figure 2.7. *Impact of the fluid to the blade.*

In (1), the entrance:

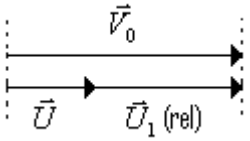

In (2), the exit:

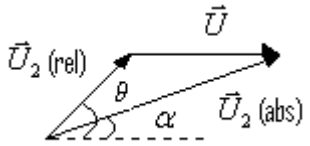

$$\vec{U}_{2,abs} = (U_2 \cos\theta + U)\hat{i} + (U_2 sen\theta)\,\hat{j}$$
$$\vec{U}_{1,abs} = V_0\hat{i}$$

Using the Bernoulli equation $\left|\vec{U}_{1,rel}\right| = \left|\vec{U}_{2,rel}\right|$ and because there is no exchange of work for a mobile observer (a observer who is in the wheel) this is equality is also fulfill $\left|\vec{U}_{1,abs}\right| = \left|\vec{U}_{2,abs}\right|$. Applying the first theorem of Euler to the volume already defined in the Figure 2.6 and assuming that the volume of flow which enters and exits in that volume is $q_m = \rho\sigma_0 V_0$

$$\vec{P} + \vec{G} = \dot{\vec{M}}_2 - \dot{\vec{M}}_1 \tag{2.43}$$

where $\vec{P}$ are the intrinsic force that act in the surface of the fluid mass and $\vec{G}$ are the force as a result of the action of the outside field (gravitational field). $\dot{\vec{M}}_2$ and $\dot{\vec{M}}_1$ are the amount of fluid which exit or enter in the volume

$$\dot{\vec{M}}_1 = q_m\vec{V}_0 = q_m V_0\hat{i} \tag{2.44}$$

$$\dot{\vec{M}}_2 = \iint_{A_2} \vec{U}_{2,abs}(\rho\vec{U}_{2,abs})d\vec{A}_2 = q_m\left[(U_2\cos\theta + U)\hat{i} + U_2 sen\theta\hat{j}\right] \tag{2.45}$$

Then,

$$\vec{R}_h = \dot{\vec{M}}_2 - \dot{\vec{M}}_1 = q_m\left[(U_2\cos\theta + U)\hat{i} + U_1 sen\theta\hat{j}\right] - q_m V_0\hat{i} = q_m(V_0 - U)\left[(\cos\theta - 1)\hat{i} + sen\theta\hat{j}\right] \tag{2.46}$$

$$\vec{R} = -\vec{R}_h = q_m(V_0 - U)\left[(1 - \cos\theta)\hat{i} - sen\theta\hat{j}\right] \tag{2.47}$$

where $\vec{R}_h$ is the reaction in the fluid and $\vec{R}$ is the reaction in blade. If the turbine is a Pelton and the blade is symmetric the component $\hat{j}$ cancel itself and the result would be

$$R = \rho A_0 V_0 (V_0 - U)(1 - \cos\theta) \tag{2.48}$$

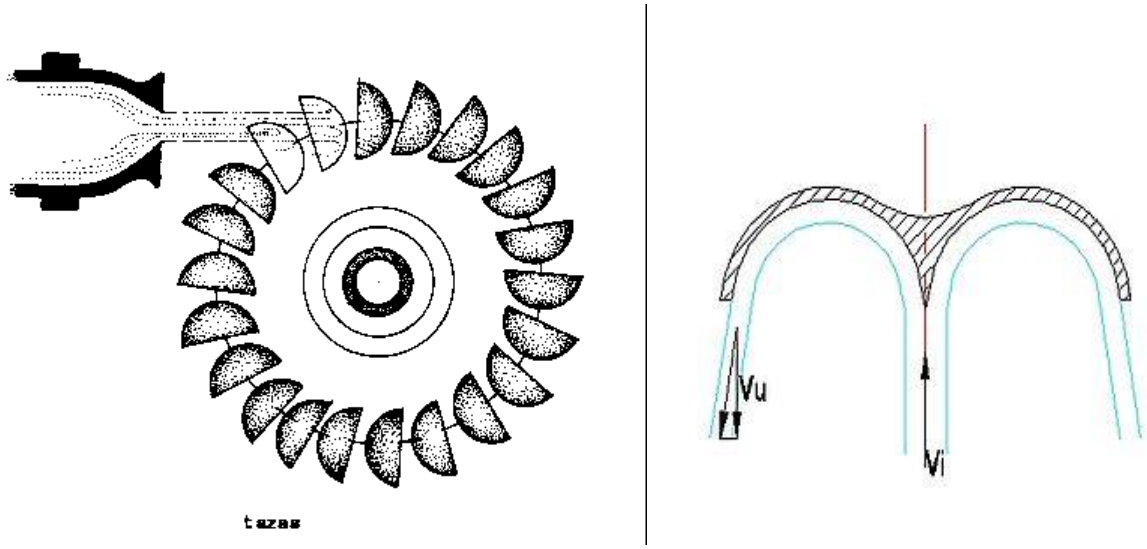

Figure 2.8. *Pelton Turbine.*

Accordingly to this the useful power would be

$$P_{useful} = R \cdot U = \rho A_0 V_0 (V_0 - U)(1 - \cos\theta) U \tag{2.49}$$

The maximum power available for a fix tangential speed U

$$\frac{dP}{dU} = \rho A_0 V_0 (1 - \cos\theta)\left[(-U) + (V_0 - U)\right] = 0 \tag{2.50}$$

$$V_0 - 2U = 0 \tag{2.51}$$

$U = \frac{V_0}{2}$ is the tangential speed for the maximum power useful of the blade.

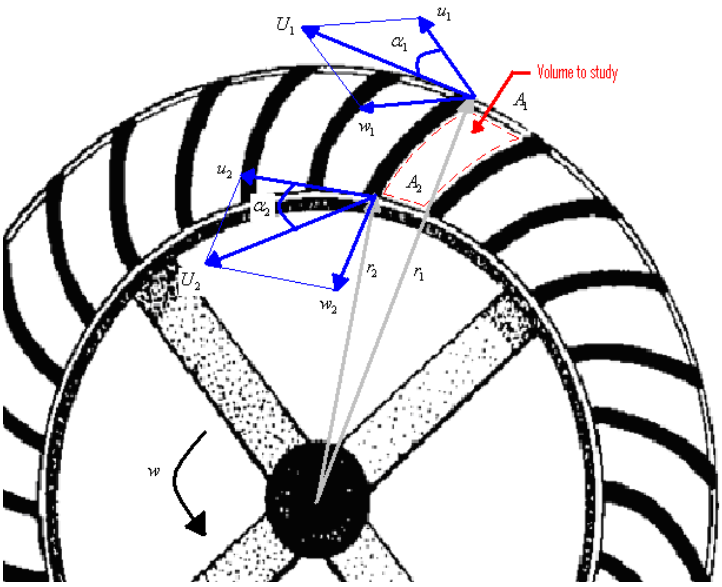

Figure 2.9. *Velocity triangles in the blade of a turbine.*

The turbines are hydraulic machines which extract energy from the fluid to transform them in mechanic which in the future could be obtained into electric. The blades of the turbine are located between two cylindrical surfaces, one with radio r_1 and the other with r_2 . The fluid enters through the outside surface r_1 and goes away through the outside surface r_2. The force R the fluid produce through the volume to study is the one which produce the momentum $C_1 = r \times R$.

In the entrance A_{11}: $U_1 = u_1 + w_1$ where $u_1 = \omega \cdot r_1$

In the exit A_{22}: $U_2 = u_2 + w_2$ where $u_2 = \omega \cdot r_2$

The momentum in the volume to study is

$$C = -C_h = r_1 \times (A_{11} p_1 \hat{n}_1 + q_m U_1) - r_2 \times (A_{22} p_2 \hat{n}_2 + q_m U_2) \tag{2.52}$$

Is also important to take into account that the positional vectors r_1 r_2 have the same direction as the $\hat{n}_1$ and $\hat{n}_2$ which are the unit normal vector of the surfaces A_{11} and A_{22} respectively (Earl Logan, JR. 1981).

$$r_1 = -r_1 \hat{n}_1 \tag{2.53}$$

$$r_2 = -r_2 \hat{n}_2 \tag{2.54}$$

For that reason the momentum of the pressure forces are null, the vectorial product of two vectors with the same direction is cero

$$r_1 \times F_1 = r_1 \times A_{11} p_1 \hat{n}_1 = 0 \tag{2.55}$$

$$r_2 \times F_2 = r_2 \times (-A_{22} p_2 \hat{n}_2) = 0 \tag{2.56}$$

So the momentum in the volume of study is

$$C_1 = q_m (r_1 \times U_1 - r_2 \times U_2) \tag{2.57}$$

To calculate the module of the momentum

$$C_1 = q_m (r_1 U_1 \cos\alpha_1 - r_2 U_2 \cos\alpha_2) \tag{2.58}$$

The mechanic power useful able to transmit to the blades is going to be the result of multiplying the momentum and the angular velocity

$$P_{useful} = C_1 \cdot \omega \tag{2.59}$$

$$P_{useful} = q_m \left[u_1 U_1 \cos\alpha_1 - u_2 U_2 \cos\alpha_2 \right] \tag{2.60}$$

Finally is well known that not all the power absorbed by the fluid is the useful power obtained for the mechanical use. In order to check the efficiency of the hydraulic turbine we have to calculate the output of the turbine by rewriting equation 2.60

$$P_{useful} = \rho Q \left[u_1 U_1 \cos\alpha_1 - u_2 U_2 \cos\alpha_2 \right] \tag{2.61}$$

The total power absorbed by the fluid is

$$P_t = \gamma Q H_n \tag{2.62}$$

The efficiency of the turbine is shown by the relationship between both powers

$$\eta = \frac{P_{useful}}{P_{total}} = \frac{\gamma Q \left[\frac{1}{g} (u_1 U_1 \cos\alpha_1 - u_2 U_2 \cos\alpha_2) \right]}{\gamma Q H_n} = \frac{u_1 U_1 \cos\alpha_1 - u_2 U_2 \cos\alpha_2}{g H_n} \tag{2.63}$$

According to the equation 2.63 the efficiency of the hydraulic system is dependant of numerous factors such as density, flow and tangential velocity. The modification of these factors by changing the liquid or the pressure inside the system could increase the efficiency of the system (Esteban, G. et al. 2006).

2.3. Wireless sensor networks

A wireless sensor networks consists of spatially distributed autonomous sensors to cooperatively monitor physical or environmental conditions, such as temperature, sound, vibration, pressure and motion. Recent developments in combining sensors, microprocessors, and radio frequency (RF) communications hold the potential to revolutionize the way we monitor and maintain critical systems. These sensors answered to the problem of the amount of dead batteries that should be change in order to operate indefinitely without the need for battery maintenance. In the future, huge amount of wireless sensors may become deeply embedded within machines, structures and the environment. As a result of this, it will be very difficult to change this amount of dead batteries. The idea is to create a new class of devices that will be battery-free and thus enable applications that would have been prohibitively expensive due to the maintenance cost of eventual and repeated battery replacement.

On the other hand, the major concerns in the current sensing network development community are the long-term reliability and sources of power. Other concerns are the abilities of the sensing systems to capture local and system-level responses. Therefore, an integrated systems engineering approach to the damage detection process and regular, well-defined routes of information dissemination are essential (G.Park et al. 2007).

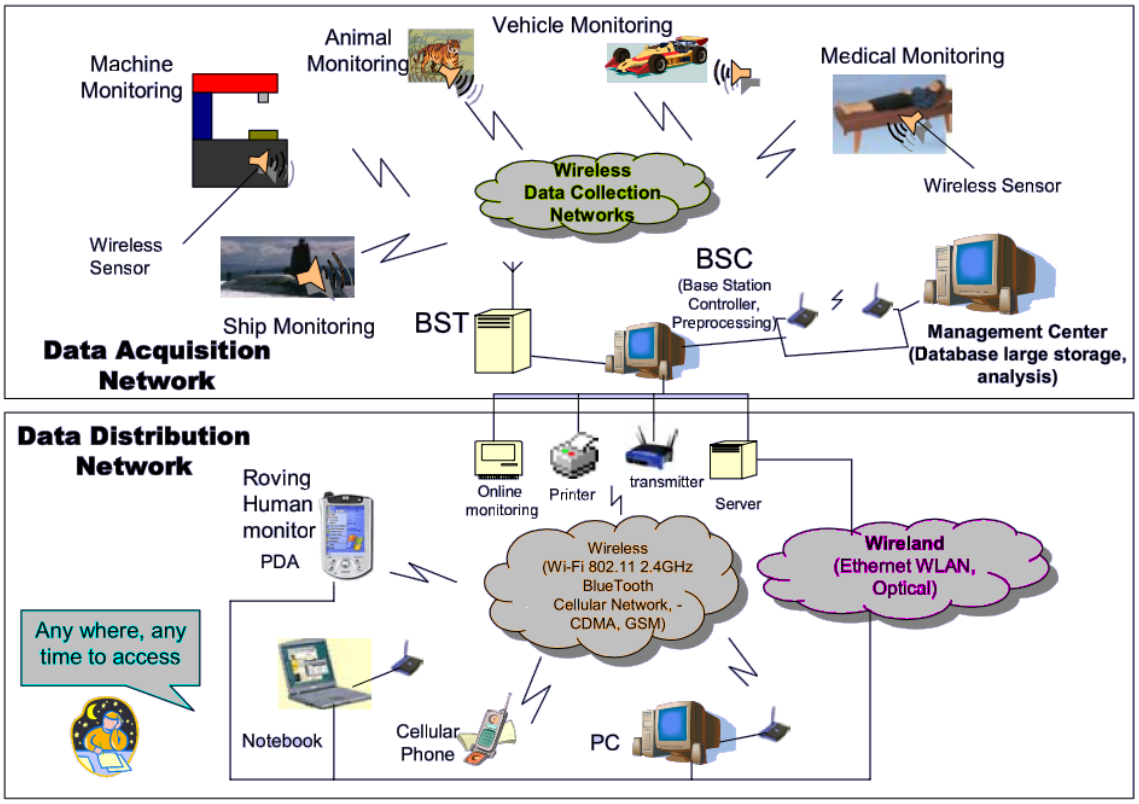

Figure 2.10. *Data acquisition and distribution networks.*

Detecting the relevant quantities, monitoring and collecting the data, assessing and evaluating the information, formulating meaningful user displays and performing decision-making and alarm functions are the responsibilities for the wireless sensor networks. Figure 2.10 shows the complexity of wireless sensor networks, which generally consist of data acquisition network and a data distribution network, monitored and controlled by a management center. Sensor networks are the key to gathering the information by smart environments, whether in buildings, utilities, industrial, home, shipboard, transportation system automation, etc. In such applications, running wires or cabling is usually impractical and a sensor network is required that is easy and fast to install and maintain (F.L. Lewis, 2004).

2.3.1. Types of wireless sensors

2.3.1.1. IEEE 1451 and Smart Sensors

There are many manufactures and many networks on the market today. It is too costly for manufactures to make special transducers for every network on the market. Different components made by different manufactures should be compatible. Therefore in 1993 the IEEE and the National Institute of Standards and Technology (NIST) began work on a standard for Smart Sensor Networks and the result was the IEEE 1451.

The objective of this standard is to make it easier for different manufactures to develop smart sensors and to interface those devices to networks. A major outcome of IEEE 1451 studies is the formalized concept of a Smart Sensor. A Smart sensor is a sensor that provides extra functions beyond those necessary for generating a correct representation of the sensed quantity. Objectives for smart sensors include moving the intelligence closer to the point of measurement, making it cost effective to integrate and maintain distributed sensor systems and creating a confluence of transducers, control, computation, and communications towards a common goal (F.L. Lewis, 2004).

2.3.1.2. Transducers

The term transducer is often used in place of the term sensor. Transducers are defined as elements that when subject to physical change experience a related change. A transducer is a device that converts energy from one domain to another, as shown in the Figure 2.11 quantity to be sensed into a useful signal that can be directly measured and processed. (W. Bolton, 2003)

Figure 2.11. *Transducer.*

The different sensors and transducers can be divided as, mechanical sensors, magnetic and electromagnetic sensor, thermal sensors, optical transducers, chemical and biological transducers and the acoustic sensors.

2.3.3.3. Sensors for Smart Environments

These sensors are divided depending of the physical properties, motion properties, contact properties, presence or even identification. There are lots of companies that offer these kind of sensors and there are suitable for many wireless network applications.

2.3.2. Areas of applications

Energy harvesting technologies is an alternative because it generates power from the surrounding environment and it uses green energy sources that require no maintenance or replacement. Moreover, there are several areas of applications that are subsequently going to be explained.

2.3.2.1. Automotive

Nowadays most part of the cars have huge amount of sensors all over the car as show the Figure 2.12 and some of them are located in places where batteries are difficult to change so the energy harvesting provides this sensors energy without the need of a battery. Furthermore, is interesting the possibility to reduce the fuel consumption. The concern about the climate change and the rise in the petrol price has increased the demand of sustainable clean technologies and the sellers of hybrids cars or vehicles which incorporate energy harvesting technologies.

Figure 2.12. *Piezoelectric sensor placement in future automobiles.*

In military vehicles the sophisticated communication system, online vehicle diagnostic devices and self protection techniques are enough consuming devices. They open the door to the energy harvesting technologies in order to reduce the amount of fuel used. Moreover it also reduces operating costs, soldier safety and even increase the vehicle travel speeds over rough terrain.

2.3.2.2. Air space

In the air space is common to use the photovoltaics cells which look similar to solar panels but they work in a different way. Photovoltaics panels convert the sunlight directly into electricity, and a example of this is a solar powered calculator powered by conentional silicon photovoltaics. Space vehicle where the gallium arsenide, germanium and other thin films together in the photovoltaics are able to obtain greater efficiency than conventional silicon photovoltaics can achieve. The greater efficiency and thin film construction mean less weight and size permitting reduced launch costs or additional payloads in a satellite. The company Boeing spectrolab is focus on this and they can convert 40.7% of the sun energy into electricity (Boeing Spectrolab, 2009).

2.3.2.3. Medical

Human body contains enormous quantities of energy, the average adult has as much energy stored in fat as a one-ton battery. That energy fuels our everyday activities, but it would be quiet interesting if those actions could in turn run the electronic devices

we rely on. In medical implants, medical devices deployed inside the body are vital to the life and well being of the patient. The problem is that without electricity these devices cannot function, so vibration energy harvesting can use the patient's own body movement and heartbeat to provide power for these life saving devices. These devices include cochlear implants, artificial retinas, electrical neuro-stimulators, automated wireless alarm signaling, advanced sensors which are called "laboratories-on-a-chip". While small size opens the door to previously unattainable applications, there are other factors, such as packaging for structural soundness and harsh environment, and power requirements which may limit the feasibility of some applications (Priya, S. & Inman, D. 2009).

In December 2009 was created a body microgenerator that converts energy from the heartbeat into power for implanted medical devices. The Self-Energizing Implantable Medical Microsystem (SIMM) microgenerator harvest energy by using differential pressure within the chambers of the heart to help augment the existing battery for implanted medical devices, such as cardiac pacemakers and implanted cardioverter defibrillators.

2.3.2.4. Construction

Construction is another important area where a lot of energy is involved in the movement of buildings and bridges due to the wind. The movement produces vibration and it is possible to harvest energy with the creation of a reference point and with an inertial mass it is able to translate the relative displacement between the vibration source and this inertial mass into electrical energy by a mechanical to electrical converter.

Figure 2.13. *Monitoring sensors in a bridge.*

Recently, sudden structural failures of large bridge spans, such as the Interstate 35W Bridge in Minneapolis, and the Chan Tho Bridge in Vietnam have resulted in the tragic loss of lives. With the wireless sensor network is possible not only to harvest energy but to monitoring the structure of the bridge in order to control and maintain it. The elimination of the long runs of wiring from each sensor location to facilitate the installation and the implementation will be an important advantage. Using the energy produced by the vibration of the structure is achievable to power the monitoring sensors because these sensors are placed usually in difficult access locations and these make difficult to change the battery periodically.

2.4. Different parts to harvest energy in a vehicle

2.4.1. Suspension

Piezoelectric patches will be attached and embedded into the leaf spring of a vehicle suspension as is shown in the Figure 2.14. When the spring is strained due to road vibrations, it strains the attached piezoelectric patch which produces an electric charge separation at the crystal lattice. The resultant electric potential across the piezoelectric patch can be transformed into useful power designing the proper electrical circuitry.

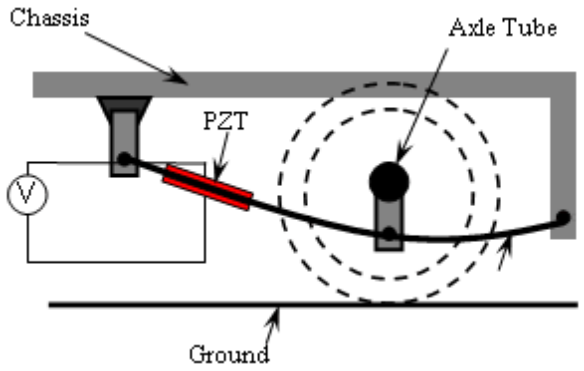

Figure 2.14. *Schematic of a piezoelectric vibration-based energy harvester.*

Under optimal operating conditions, piezoelectric materials can produce up to 0.2 $Watts$ per $sq-cm$. In addition to acting as an additional power source, this approach provides a passive damping technique to reduce or adapt vehicle vibrations (Automotive Research Center, 2009).

2.4.2. Brakes

It is well known that in the last few years Kinetic Energy Recovery Devices or KERS has played an important role in the car industry and especially in the F1. In the F1 this devices use some of the waste energy from the braking process into more useful types of energy which can then be used to give the cars a power boost. For the commercial cars the idea will be the reduction of fuel instead of the increase of power. There are different types but the most common one is the electronic KERS that is the one used in the F1 by Ferrari, Renault, Toyota and Red Bull.

As is shown in the Figure 2.15 when the car brakes there is a proportion of the rotational force captured by a electric motor-generator. This motor-generator converts the kinetic energy into electrical which is the stored in batteries. When the driver presses the boost button the electrical energy in the batteries powers the motor-generator which puts an extra 85bhp into the engine.

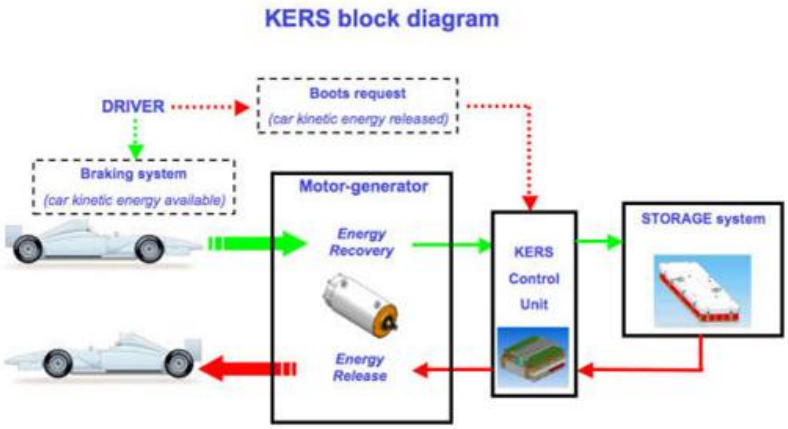

Figure 2.15. *Box diagram explanation about KERS.*

The toughest part is how to store the electrical energy and in the most part of the cases use a lithium battery. However, a cooling system is required because the battery gets hot while is charging.

2.4.3. Cranshaft

The properties of magnetostrictive materials can be applied to generate electricity for in-vehicle power budgets. The proposed generator utilizes this smart material to directly transform mechanical strain into a magnetic field. When magnetostrictive materials are subjected to time-varying strain, they produce a time varying magnetic field which can be transformed into electrical energy using Faraday's law. In optimal operation, a 50 mm long magnetostrictive rod with a diameter of 12mm can produce up to 100Watts.

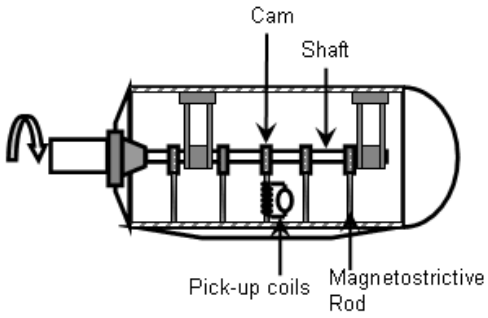

Figure 2.16. *Schematic of a Magnetostrictive generator.*

This innovative concept may supplement traditional alternators/generators and reduce the cost maintenance complexities of power generation. Another advantage is that the generators efficiency can be maximized at low rotational speeds. Therefore, a magnetostrictive generator can be retrofitted on the engine crankshaft to act as a substitute generator which boosts the power efficiency especially at low engine speeds. Furthermore, the generator can be produced at small sizes with very high efficiency and also can operate at elevated temperature (Automotive Research Center, 2009).

2.4.4. Solar panels in the roof

Solar cars can accomplish photovoltaics cells (PVC) which are the components in solar paneling that convert the sun's energy into electricity. They are made up of semiconductors, usually made of silicon that absorbs the light. The sunlight's energy then frees electrons in the semiconductor, creating a flow which generates electricity that powers the battery or the specialized car motor in solar cars.

Figure 2.17. *Solar panels implemented in a car.*

Nowadays the main aim for car manufactures is to cool the cabin when the car is parked and the interior temperature rises using these solar panels.

2.5. Other applications.Backpacks

Researchers have begun to investigate new sources and ways to harvest energy, one of them is referred to the backpack. The idea is that the backpack can generate electrical energy from the differential forces between the wearer and the pack during walking. In 2005 Rome et al investigated the design of a backpack that could convert mechanical energy from the vertical movement of carried loads to electricity. The backpack was designed in a way that a linear bearing and a set of springs suspended the load relative to a frame and shoulder harness as is shown in the Figure 2.18. The relative motion was then converted to electrical energy using a rotary electric generator with a rack and pinion.

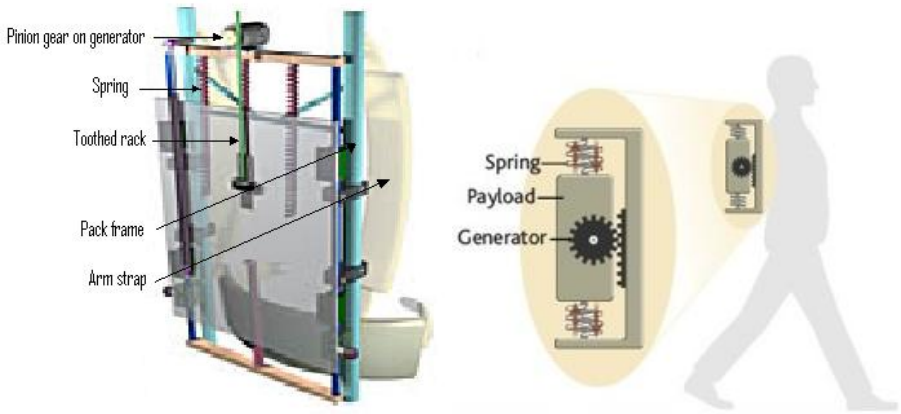

Figure 2.18. *Different parts of the backpack and how it works.*

Many of the systems invented are compatible with the energy present around a worker or a soldier but few of them are comfortable for the user and not interfere with its gait. Also is important to design a system such that the power-harvesting backpack provides no additional stress or load to the wearer over that of a conventional backpack. There are two systems to harvest the dynamic energy from a backpack, one is the piezoelectric polymer polyvinylidene fluoride (PVDF) and the other is the mechanically amplified stack actuators.

The PVDF bulk material is widely available and is low cost. However, it requires processing to obtain piezoelectric properties. In order to make the backpack as close to a typical design as possible, the fabrics straps are to be replaced with a PVDF polymer strap. As the soldier walks with the backpack, the differential forces between wearer and backpack would be transferred to the polymer straps which then convert the applied force to electrical energy. The second energy harvesting system presented here uses piezoelectric stack actuators for energy harvesting. Stack actuators are not common for the power harvesting applications because of their high stiffness which makes straining the material difficult under typical ambient vibration levels. This problem can be solved using the mechanically amplified stack actuator which employs a simple kinematic

design to transform the low force in the strap to a high force at the piezoelectric stack (Priya, S. & Inman, D. 2009).

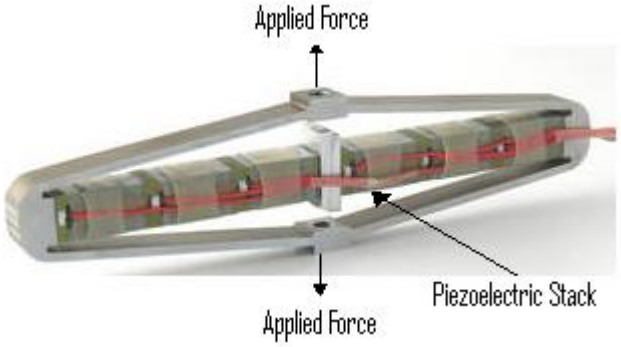

Figure 2.19. *Mechanically amplified stack actuator*.

The results using this PVDF polymer strap showed that 45.6 mW of continuous power could be obtained from the PVDF polymer system, while 16 mW could be obtained by the amplified stack.

3. THEORICAL IMPLEMENTATION IN THE VEHICLE SUSPENSION

In the theorical background there is an overview of the different principles or methods that can be used to harvest energy. This section focuses in the implementation of those methods in the vehicle suspension. The most interesting methods for the implementation in a vehicle suspension are: piezoelectric, electromagnetic and hydraulic. The idea is to compare those methods taking into account the effectiveness, simplicity, durability and resistance.

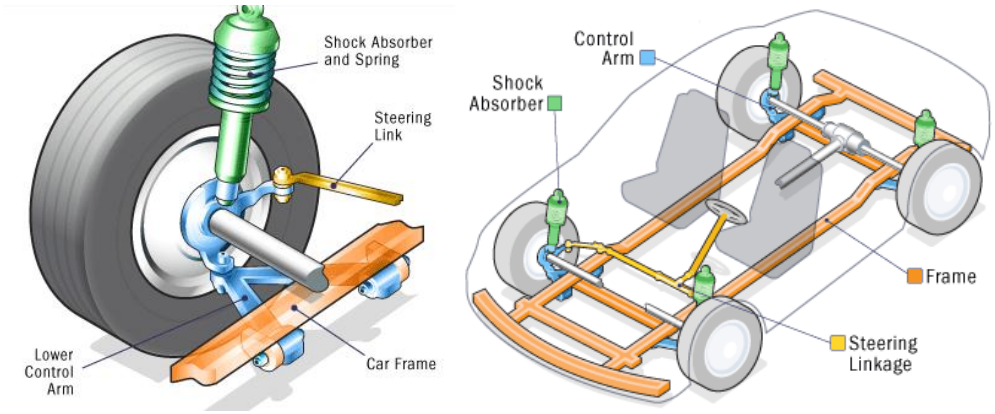

Figure 3.1. *Overview of the suspension in a vehicle.*

Suspension geometry is a broad subject which focuses on how the unsprung mass of a vehicle is connected to the sprung mass. These connections not only dictate the path of relative motion, but they also control the forces that are transmitted between them (Milliken & Milliken, 1995). The implementation is to modified or rebuilds the shock absorber depending on the method used. The result is a suspension which can not only damp but recover energy from the movement of the shock absorber. Before going through the different possibilities to harvest energy is interesting to know how the car suspension works.

The suspension is a very important part inside a vehicle for the reason that all the power generated by a piston engine is useless if the driver can not control the car. The main aim of the suspension is to maximize the friction between the tires and the road surface, to provide steering stability with good handling and to ensure the comfort of the passengers. If a road were perfectly flat, with no irregularities, suspensions would not be necessary. A bump in the road causes the wheel to move up and down perpendicular to

the road surface and the car wheel experiences a vertical acceleration as shown in Figure 3.2. If there is no suspension all the wheel vertical energy is transferred to the frame, which moves in the same direction so the wheel can lose contact with the road completely.

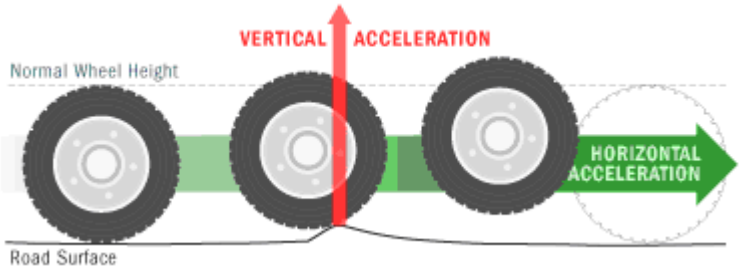

Figure 3.2. *Wheel through a bump.*

In order to avoid this problem a system that absorbs the energy of the vertically accelerated wheel is needed, allowing the frame and body to ride undisturbed while the wheels follow bumps in the road.

Every car suspension is based on a spring and a shock absorber as shown Figure 3.1. There are different types of shock absorbers but one of the most common is the hydraulic shock absorbers. In the standard twin-tube shock absorber design, a piston slides inside an oil-filled cylinder. The upper mount is connected to a piston rod while the lower mount is connected to the base valve. Calibrated holes in the piston allow oil to pass between the upper and lower part of the cylinder thereby damping the oscillation of the spring. When the piston moves up and down forced the oil through the holes and the piston rod moves in and out of the tube. As it moves in and out, the rod changes the volume available to the oil. When the volume is reduced, there is momentarily an excess of oil: this excess is forced back in the reserve tube through the base valve. Finally when the rod moves out again, it creates a vacuum and the volume of oil equivalent to the displaced rod is drawn through valves in the piston.

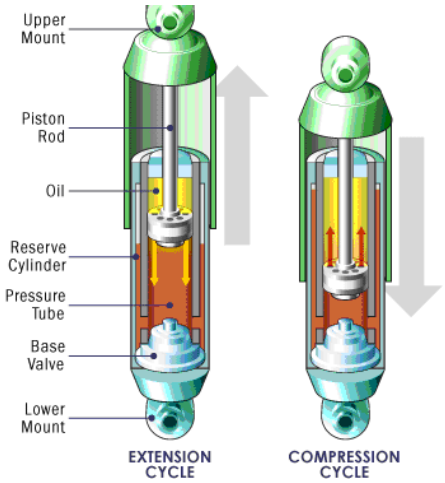

Figure 3.3. *Twin-tube shock absorber.*

Modern shock absorbers are velocity-sensitive which means that, the faster the suspension moves, the more resistance the shock absorber provides. Anti-sway bars are an important component in a vehicle suspension used along with shock absorbers to give a moving automobile additional stability. An anti-sway bar is a metal rod that spans the entire axle and effectively joins each side of the suspension together.

3.1. Piezoelectric

The piezo will be located in the top part of the piston. Subsequently, when the outer tube goes into the shell at the end of the trajectory it impacts with the piezo getting the voltage difference. As much as bumps there are in the road more energy can be produced. One disadvantage is that the bump must not be too big because the outer tube could reach the top part of the shell destroying the piston. On the other hand, if the dashpot is soft there will be risk of breaking it.

Furthermore in order to improve the effectiveness of the piezo a multiplayer PZT stack is needed. The piezo is going to work in the thickness mode (d-33 effect) and stacking of several layers towards a multiplayer structure increases equivalently the total stroke. In practice, axial strain rates up to 2 % of the stack's length can be achieved under certain conditions (Pickelmann D. L.GmbH, 2003).

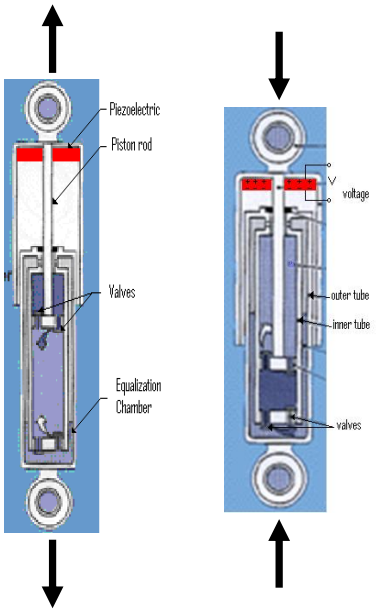

Figure 3.4. *Piezoelectric inside the twin-tube shock absorber.*

Piezo actuators are divided between low voltage and high voltage. For the selection of the piezoelectric to introduce in the shock absorber, a comparison of materials and dimension, electrical properties, temperature ranges, vacuum compatibility, reliability and mounting procedures is needed. Low voltage actuators are mostly used as small medium sized elements with cross sections typically up to 10×10. Larger cross sections lead to a dramatic increase of costs but low voltage actuators become cheap in large quantities. Manufacturing of actuator prototypes of non-standard size and performance is much easier for high voltage elements than with low voltage elements and all kinds of PZT materials can be easily implemented. Low voltage elements use a larger number of thinner active layers compared to high voltage elements to get the same active stack's length. This result in an equivalently higher electrical capacitance, but the required charging power to drive a stack is the same in both cases. The operation both of high voltage and low voltage actuators is possible without problems in normal vacuum.

According to the reliability the main problems are mechanical stress and fatigue. To avoid this L. Pickelmann introduced in 1970ies the electrode wrapping technology where the stacks withstand high frequency cycling. In the mounting procedures the actuators with casing are much more robust against mechanical impacts and environmental influences than bare stacks which are mounted using only end-faces. Ring actuators prevent any mechanical damage or attack of unwanted substances to the coated inner side of the ring.

Finally, in order to select a stack actuator for this particular operation the high voltage stack actuator PSt 1000/25/…is chosen

Type	max. Stroke µm	length L mm	el. Capacitance µF	stiffness N / µm	resonance frequency kHz
PSt 1000/25/5	12/7	9	140	1800	60
PSt 1000/25/15	25/17	18	350	900	40
PSt 1000/25/40	55/40	36	800	450	25
PSt 1000/25/60	80/60	54	1250	300	20
PSt 1000/25/80	105/80	72	1700	200	15

Figure 3.5. *Different types of stack actuators for the same PSt 1000/25/.*

For the PSt 1000/25/… the maximum load is 35000N the maximum force generation is 25000N (Pickelmann D. L. GmbH, 2004).

Once the piezoelectric is strained metal electrodes are deposited on opposite faces of the piezoelectric crystal and the capacitance C of the piezoelectric material between the plates is

$$C = \frac{\varepsilon_0 \varepsilon_r A}{t} \tag{3.1}$$

where ε_r is the relative permittivity of the material, A is the area and t its thickness. The charge is $q = Cv$ where v, is the potential difference produced across a capacitor, then

$$v = \frac{S \cdot t}{\varepsilon_0 \varepsilon_r A} F \tag{3.2}$$

where the S is a constant termed the charge sensitivity and it depends on the material concerned and the orientation of its crystals. Instead of using the equation 3.2, equation 3.3 is used, where $S_v = S / \varepsilon_0 \varepsilon_r$ and is called voltage sensitivity factor. For the barium titanate it is 0.011V/mPa and for quartz is about 0.055V/mPa. (W. Bolton, 2003)

$$v = S_v t p \tag{3.3}$$

To get the amount of energy we are going to harvest in one bump, the pressure of the impact and thickness of the stack is needed. The normal weight for a car is $1813 kg$ and the distribution is 51% for the front wheels while 49% for the back wheels. To get an idea how much energy can harvest for the front wheel, the force is

$$\frac{1813 \cdot 0{,}51}{2} = 462{,}315$$

The diameter is $25{,}5 mm$ and the area $510{,}070\, mm^2$ so the voltage for the PSt 1000/25/40 is

$$v = \frac{0.055 \cdot 36 \cdot 462{,}315 \cdot 9{,}8}{510{,}070 \times 10^3} = \frac{8970{,}76026}{510070} = 0{,}01759 V$$

This is going to be per bump in the road.

3.2. Electromagnetic

There are already design two types of EM regenerative shocks. The first option consists of several very powerful permanent magnets mounted to the outer sleeve and a moving coil assembly mounted to a sliding armature. The coils moving in the magnetic field generate electrical power as shown in the Figure 3.6 (Gupta, A. et al. 2007). When the car passes through a bump the shock will be compressed so the permanent magnet which is inside the coil moves up inducing a current in the stator windings according to Faraday's law. The magnet of the shock consists of an inner magnet stack surrounded concentrically by a larger diameter outer magnet stack and the coil consists of an inner coil surrounded concentrically by a larger diameter outer coil.

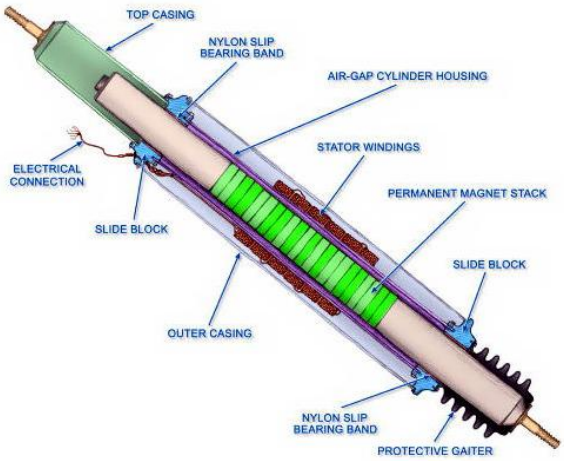

Figure 3.6. *E.M. regenerative shocks.*

For coils with $n = 8.26\,turns/mm$ moving axially with a velocity u past a stationary pole emanating flux density B_i a voltage is generated in each section of the coil according to the equation 3.4.

$$V = nhuB_i \tag{3.4}$$

where h_2 is the height of the pole ring. Again, to have an idea of the voltage that can be generated with this method we assume $B_i = 1T$ coil speed $u = 0.01m/s$ so each middle section of the outer coil will generate an open-circuit of voltage $0.169V$. Each middle section of the inner coil will produce in proportion to its smaller diameter, a smaller voltage of $0.062V$. The bottom and the top sections of each coil will generate only half these voltages. For both coils the total voltage is

$$v = 0.69V$$

Another possibility consists of a small DC motor coupled to a lever arm by a system of gears, which results in approximately six revolutions of the motor to one of the lever. (Gupta, A. et al. 2007)

It is interesting to remark that the famous maker of speakers Bose has built electromagnetic shock absorber after 24 years of secretive research. Bose system uses a linear electromagnetic motor (LEM) at each wheel as shown the Figure 3.7 instead of a conventional shock-and-spring setup (Bose suspension system, 2010).

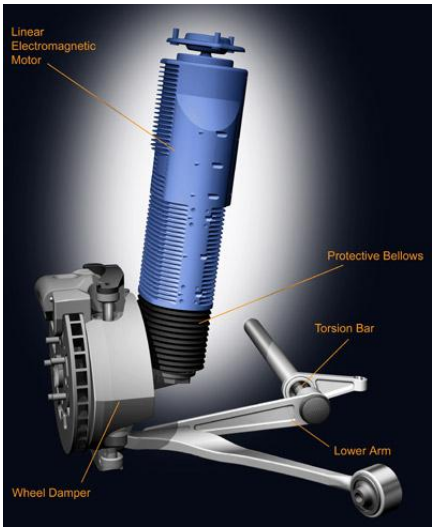

Figure 3.7. *Bose suspension system*

Amplifiers provide electricity to the motors in such a way that their power is regenerated with each compression of the system. The main benefit of the motors is that they are not limited by the inertia inherent in conventional fluid-based dampers. As a result, an LEM can extend and compress a much greater speed, virtually eliminating all vibrations in the passenger cabin. The wheel motion can be so finely controlled that the body of the car remains level regardless of what is happening at the wheel (Bart, L. et al. 2008).

3.3. Hydraulic

Energy harvesting from a vehicle suspension using a hydraulic system was developed by researchers at the Massachusetts Institute of Technology (MIT). They came up with a hydraulic system that forces fluid through a mini-turbine and attached to a electric-motor generator as shows the Figure 3.8.

Figure 3.8. *Hydraulic system for suspension energy harvesting.*

The system in the Figure 3.8 adapted from (Levant Power Corporation, 2009) consists of three parts: the piston, hydraulic motor and the electric-motor generator. In the compression cycle the left hole is closed and the fluid is pushed through the right hole impacting into a turbine. The rotation of the turbine as a result of the fluid pressure will be transformed into electrical energy. In the expansion cycle of the piston the right hole will be closed, moreover as the piston moves down a vacuum is created so the fluid that remains in the turbine sucked to the inside of the piston.

It is important that a hydraulic system contains no air bubbles. If there is an air bubble in the system, then the force applied to the piston gets used compressing the air in the bubble rather than pushing the fluid. This has a big effect in the efficiency of the system. To get an idea of the amount of energy that is possible to obtain some calculations are done.

The equations already obtain in the theorical background are difficult to use them without some previous test or measures. We need to know numerous parameters and without testing any prototype is complicated. Even though, is possible to make an approximation to calculate the electrical power the system can generate in a theoretical way. The diameter of a conventional shock absorber is around $55mm$ and the pressure inside the piston in driving conditions is more or less $350bar$. The size of the holes where the fluid flow under pressure is $10mm$

$$P_{useful} = R \cdot U = \rho A_0 V_0 (V_0 - U)(1 - \cos\theta) U \tag{3.5}$$

$$C = q_m (r_1 U_1 \cos\alpha_1 - r_2 U_2 \cos\alpha_2) \tag{3.6}$$

$$\omega = \frac{P_{useful}}{C} \tag{3.7}$$

Similarly velocity parameters U , U_1, U_2 are needed. Once we have all these values and the ω we are able to apply the equation 3.8 of an electric motor which is an approximation

$$P_{electric} = \frac{C \cdot n}{5{,}250} \tag{3.8}$$

There are some tests already done with this type of hydraulic system and the output power is from $800W$ up to $5kW$. This is the total power of the four shock absorbers, so each absorber will recover at least $200W$.

3.4. Comparison

After taking into account the implementation of the three methods now is time to compare and contrast the three methods already explained in terms of reliability, resistance, economic, efficiency, quality and easy implementation. Concerning reliability and resistance the piezoelectric method consists in fewer parts thus, is the one which is going to support better hard ambient conditions. Furthermore, less maintenance is required for it. The hydraulic system and the electromagnetic both of them have very weak parts which maintenance is required in the future.

Regarding the efficiency the hydraulic system is without any doubt the one which is able to produce more electricity but in terms of durability and easy implementation the electromagnetic device or the piezoelectric take advantage. Finally about economic part the hydraulic system is the most expensive. The mini-hydraulic turbine incorporated and the pipes which connect the turbine with the piston are expensive components that raise the price of the system. In the same way, the electromagnetic system has also numerous components for instance the permanent magnet the stator windings. On the other hand, the piezoelectric is the most simple so the final price is lower than the other ones.

A good balance of the parameters is needed for the final result. The Figure 3.9 gives an overview of the comparison between the three methods. The hydraulic system is focus mainly in the efficiency, the piezoelectric is in the opposite side more focus on economic, resistance and the electromagnetic is a mixture of both. Since this project is mainly focus on the efficiency of the system, the most interesting system to simulate is the hydraulic.

Method / Parameter	Hydraulic system	Electromagnetic	Piezoelectric
Reliability	moderate	low	high
Economic	expensive	moderate	cheap
Efficiency	high	moderate	low
Implementation	difficult	normal	easy

Figure 3.9. *Comparison between methods.*

4. SIMULATION

In this part the energy harvesting system effect to the passenger's cabin when the vehicle goes through a bump in the road are analyzed. The simulation is focus in the hydraulic system and the results are calculated using Mathcad program. The implementation of this hydraulic system is traduced theoretically in an increase in the damping factor of the system. If the damping increase the friction increase so there will be more energy available that can be recover with any of the energy harvesting system explained before. However, if the damping is so hard the system can be over damp which means that the suspension could not soften the bumps.

In the simulation a balance between both aims is done in order to know how much energy is possible to harvest without loosing the suspension properties. We will simulate four different models, starting with a simple one and complicating it to get better accuracy. Bumps of different shapes are simulated moreover parameters such as velocity and mass are change in order to observe the reaction of the system against this changes.

4.1. First Model Simulation

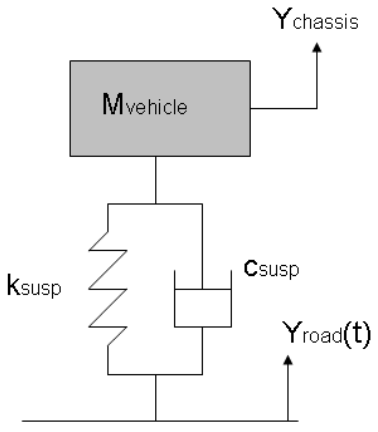

Figure 4.1. *First model of the vehicle.*

First of all is to define the variables that are needed. The c_{susp} is determined by the system. The limit is settled when the system gets over damped. As we know when a system is over damped ξ>1 so the limit is for $\xi = 1$

$$\xi = \frac{c_{susp}}{2 \cdot M_{vehicle} \cdot \omega_0} \tag{4.1}$$

where ω_0 is the natural frequency of the system. If we equal the equation 4.1 to one then we get $c_{t\max}$ which is the maximum possible damping for that system. $c_{t\max}$ is the damping for the system with the energy harvesting system.

$$\omega_0 = \sqrt{\frac{K}{M_{vehicle}}}$$

$$\xi = \frac{c_{t\max}}{2 \cdot M_{vehicle} \cdot \omega_0} = 1$$

$$c_{t\max} = 16980 Ns/m$$

For the vehicle without energy harvesting system the damping is c_{susp}

$$M_{vehicle} = 1800 kg$$
$$k_{susp} = 40000 N \cdot m$$
$$\xi_{susp} = 0.3$$
$$c_{susp} = \xi_{susp} \cdot \sqrt{M_{vehicle} \cdot k_{susp}} = 2546 N \cdot s/m$$

To get the equations of motion which are going to rule the system the freebody diagram is needed.

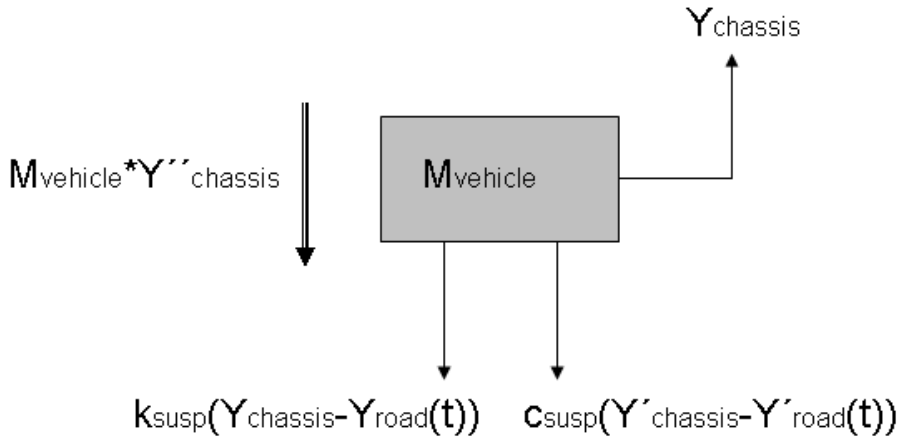

Figure 4.2. *Freebody diagram for the first model.*

Equation of motion for this system

$$M_{vehicle}\ddot{Y}_{chassis} + c_{susp}\dot{Y}_{chassis} + k_{susp}Y_{chassis} = k_{susp}y_{road}(t) + c_{susp}\dot{y}_{road}(t) \tag{4.2}$$

The contour of the bump is defined by the function $Y_{road}(x)$ and it will vary depending of the bump.

$$Y_{road}(x) = \begin{cases} \frac{1}{4}\cdot\sin(x) & / \quad if\ 0 < x < \pi \\ 0 & / \quad otherwise \end{cases} \tag{4.3}$$

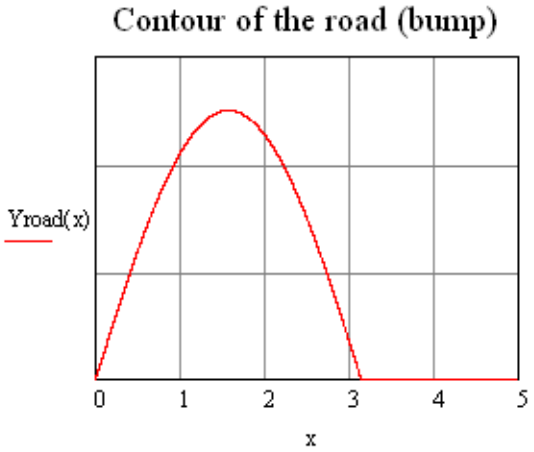

Figure 4.3. *Profile of the bump.*

The excitation force $Y_{road}(x)$ has to be converted into the time domain t to introduce it into the equation of motion and obtain the excitation force. The speed of the vehicle is $vel = 30{,}54 m/s$. As we know the formula from cinematic.

$$x = x_0 + v \cdot t \tag{4.4}$$

where x_0 is the initial displacement which is cero. Then, the equation 4.3 can be wrote as

$$y_{road}(t) = \begin{cases} \frac{1}{4} \cdot \sin(vel \cdot t) \ / \ if \ 0 < t < \frac{\pi}{vel} \\ 0 \ / \ otherwise \end{cases} \tag{4.5}$$

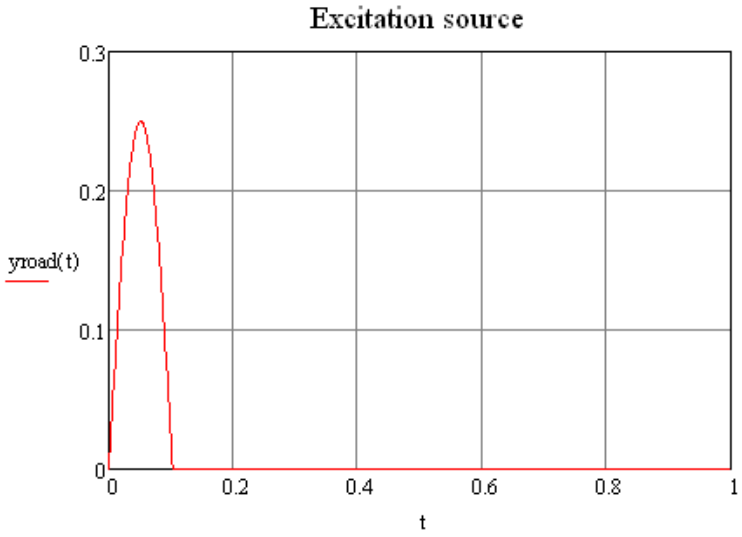

Figure 4.4. *Excitation source.*

Now is possible to calculate the forces actuating in the wheel

$$F_{force}(t) = k_{susp} \cdot y_{road}(t) + c_{susp} \cdot \dot{y}_{road}(t) \tag{4.6}$$

For obtaining the displacement and acceleration of the chassis the Runge Kutta method is used in Mathcad as follows.

$$t_0 = 0$$

$$t_{max} = 5$$

$$D(t, y) = \begin{bmatrix} y_2 \\ \dfrac{F_{force}(t) - c_{susp} \cdot y_2 - k_{susp} \cdot y_1}{M_{vehicle}} \end{bmatrix}$$

$$Invalues = \begin{bmatrix} 0 \\ 0 \end{bmatrix}$$

$$S = rkfixed(Invalues, t_0, t_{max}, 500, D)$$

$$t = S^{\langle 1 \rangle}$$

$$Y_{chassis} = S^{\langle 2 \rangle}$$

$$\dot{Y}_{chassis} = S^{\langle 3 \rangle}$$

The values of time t, displacement of the chassis $Y_{chassis}$, and velocity $\dot{Y}_{chassis}$ are stored in a vector called S. The *Invalues* are the initial conditions and the t_0 and t_{max} defined the range for the plot.

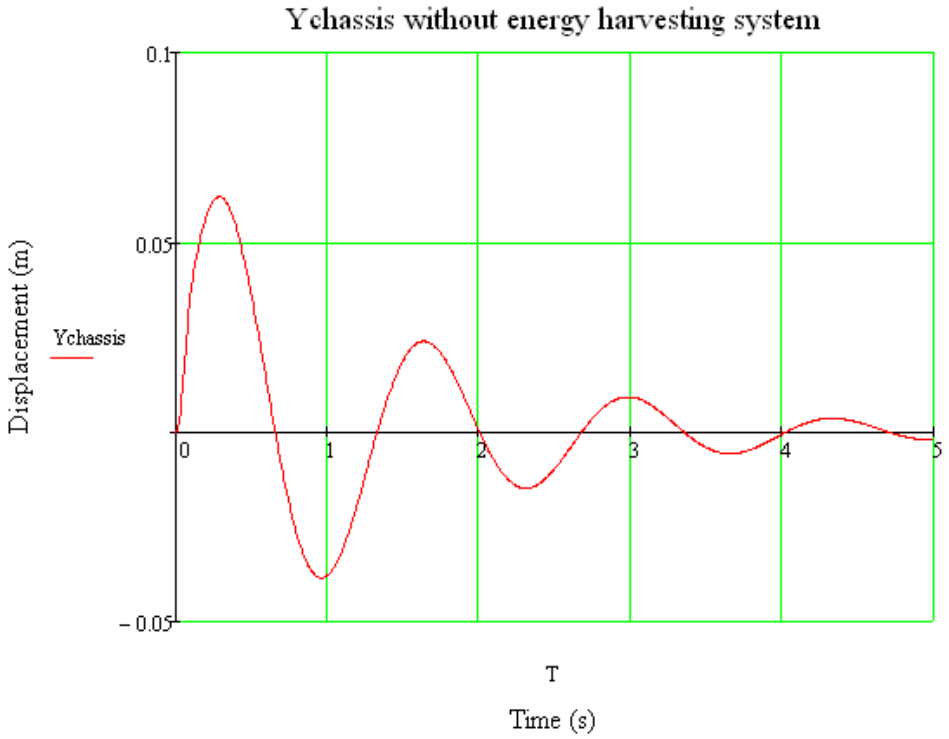

Figure 4.5. *Vertical displacement of the chassis without energy harvesting system.*

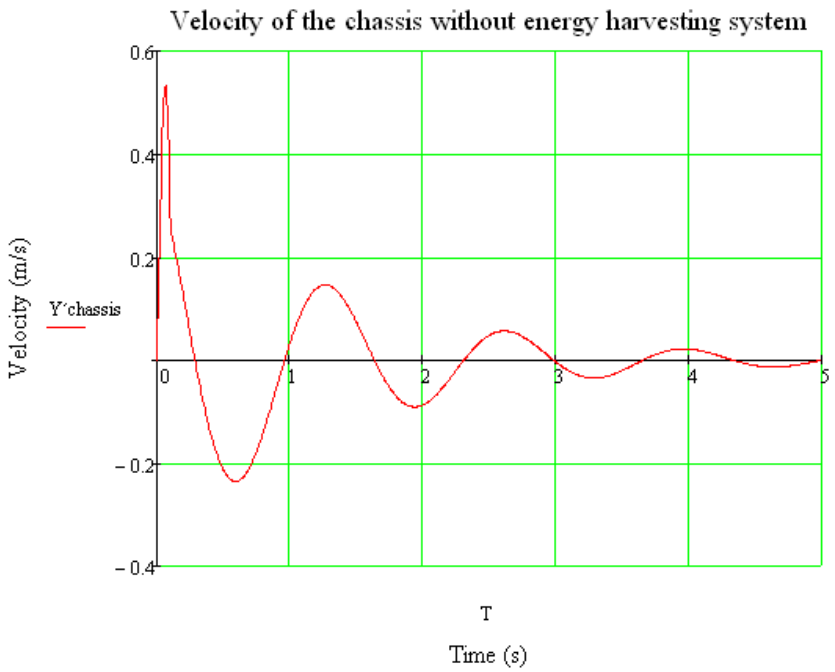

Figure 4.6. *Vertical velocity of the chassis without energy harvesting system.*

Finally, the acceleration of the chassis as a result of the bump.

$$\ddot{Y}_{chassis}(t) = \frac{F_{force}(t) - c_{susp} \cdot \dot{Y}_{chassis}(t) - k_{susp} \cdot Y_{chassis}(t)}{M_{vehicle}} \tag{4.7}$$

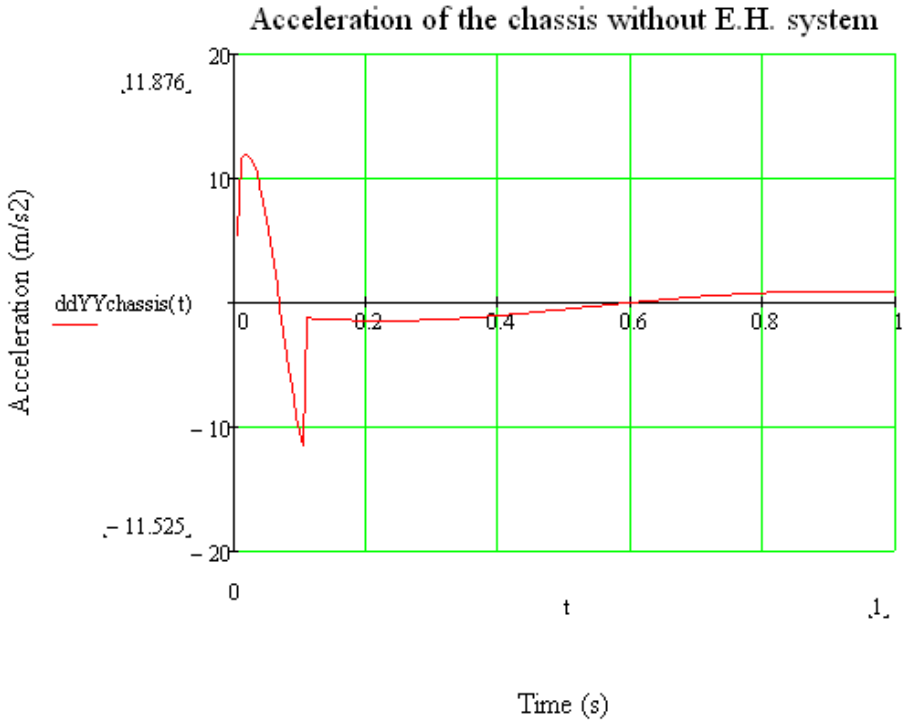

Figure 4.7. *Vertical acceleration of the chassis without energy harvesting system.*

Once the energy harvesting system is introduced in the suspension, the $C_{damping}$ of the suspension is going to increase from c_{susp} to $c_{t\max}$. As much as the damping is increased much more energy will be involved in the system so more energy will be harvested with the system. As it is said before, the maximum limit is the over-damp of the system. Therefore, the idea is to make a balance between the amount of energy is possible to harvest and the damping of the system. Moreover, special focus will be done in the accelerations, the values could not overpass human being.

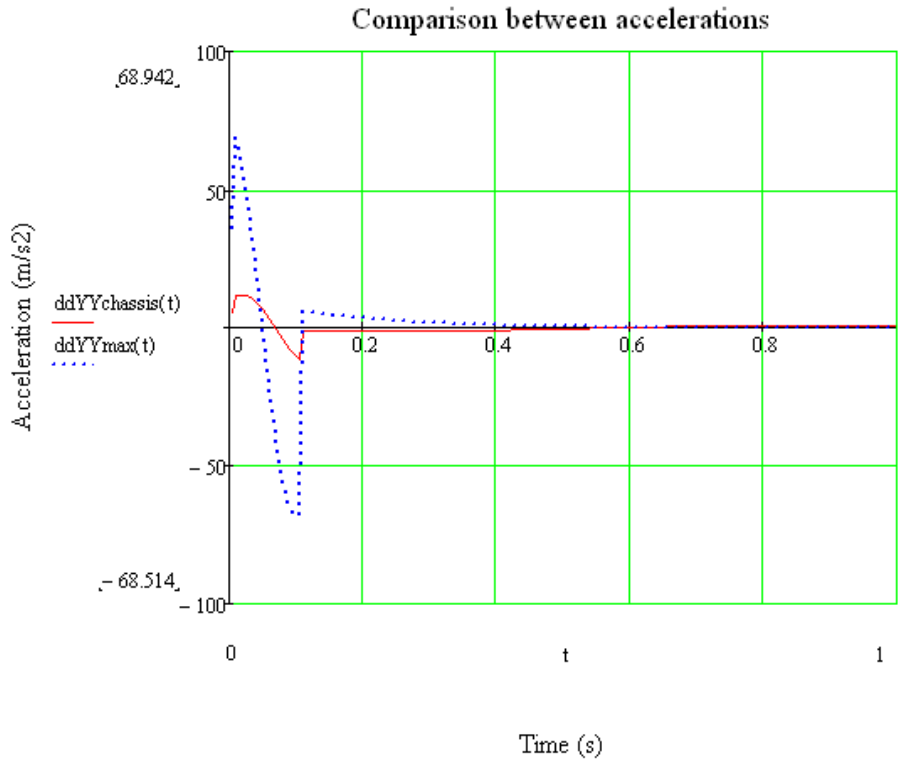

Figure 4.8. *Comparison of vertical accelerations in the chassis of the vehicle.*

In the Figure 4.8 is plotted the acceleration for the chassis without any energy harvesting system and the acceleration with the maximum damping $c_{t\max}$ just when it is over damped. However, there is another limit related to the human being that has more restriction than the first one as it showed later.

The amount of energy harvested by the system is calculated using the equation below

$$W_{total} = \int_0^t c_{t\max} \cdot (\dot{Y}_{chassis}(t) - \dot{y}_{road}(t))^2 \, dt \tag{4.8}$$

4.2. Second Model simulation

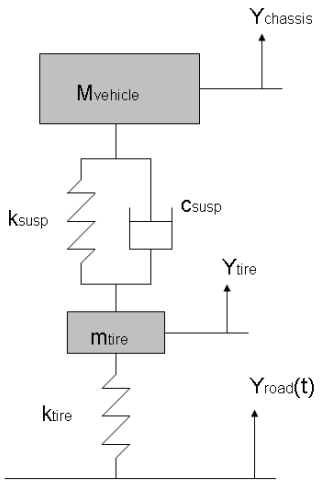

Figure 4.9. *Second model of the vehicle.*

This second model of the simulation takes into account the mass of the tire separating it from the mass of the chassis becoming a two degree of freedom system. Again, the excitation source will be the profile of the road. The free body diagram is necessary to obtain the equations of motion.

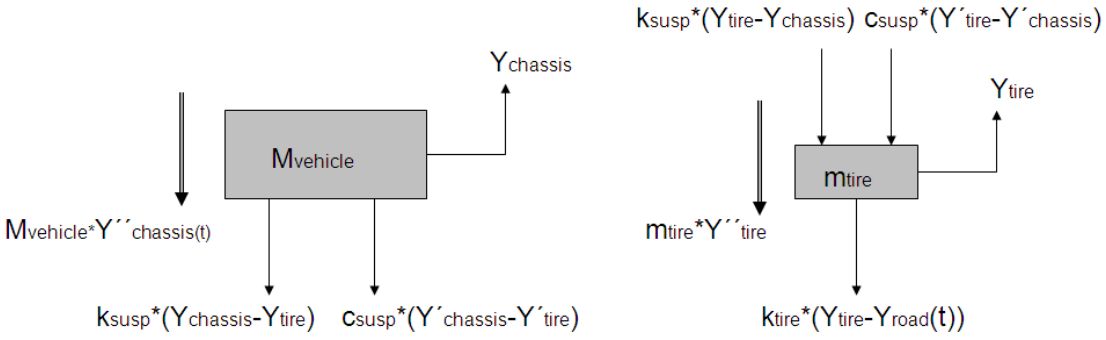

Figure 4.10. *Freebody diagram for the second model.*

The equations of motion

$$M_{vehicle} \cdot \ddot{Y}_{chassis} + c_{susp} \cdot \dot{Y}_{chassis} - c_{susp} \cdot \dot{Y}_{tire} + k_{susp} \cdot Y_{chassis} - k_{susp} \cdot Y_{tire} = 0$$

$$m_{tire} \cdot \ddot{Y}_{tire} + c_{susp} \cdot \dot{Y}_{tire} - c_{susp} \cdot \dot{Y}_{chassis} + k_{susp} \cdot Y_{tire} + k_{tire} \cdot Y_{chassis} = k_{tire} \cdot y_{road}(t) \tag{4.9}$$

The force applied to the mass of the tire is calculated in the equation 4.10

$$F_{force}(t) = k_{tire} \cdot y_{road}(t) \tag{4.10}$$

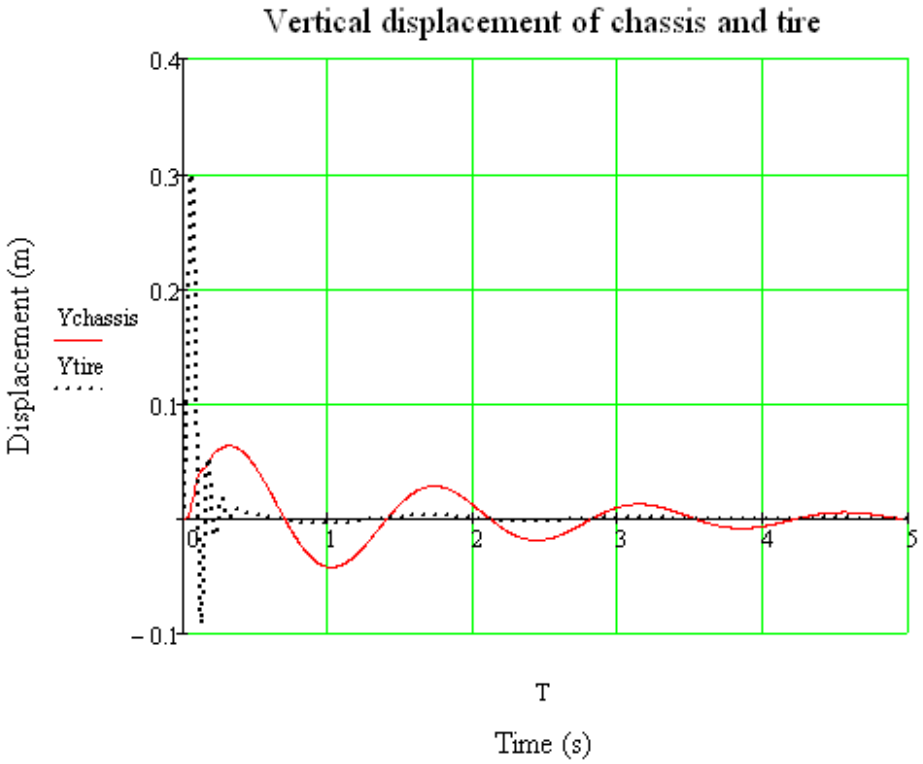

Figure 4.11. *Vertical displacement of chassis* $Y_{chassis}(t)$ *and tire* $Y_{tire}(t)$.

The accelerations are calculated as shown in the equation below

$$\ddot{Y}_{chassis}(t) = \frac{F_{force}(t) - c_{susp} \cdot \dot{Y}_{chassis} - k_{susp} \cdot Y_{chassis} + c_{susp} \cdot \dot{Y}_{tire} + k_{susp} \cdot Y_{tire}}{M_{vehicle}} \tag{4.11}$$

The Figure 4.12 shows the comparison between the acceleration for the vehicle with c_{susp} and the vehicle with $c_{t\max}$ which means that has incorporated the energy harvesting system.

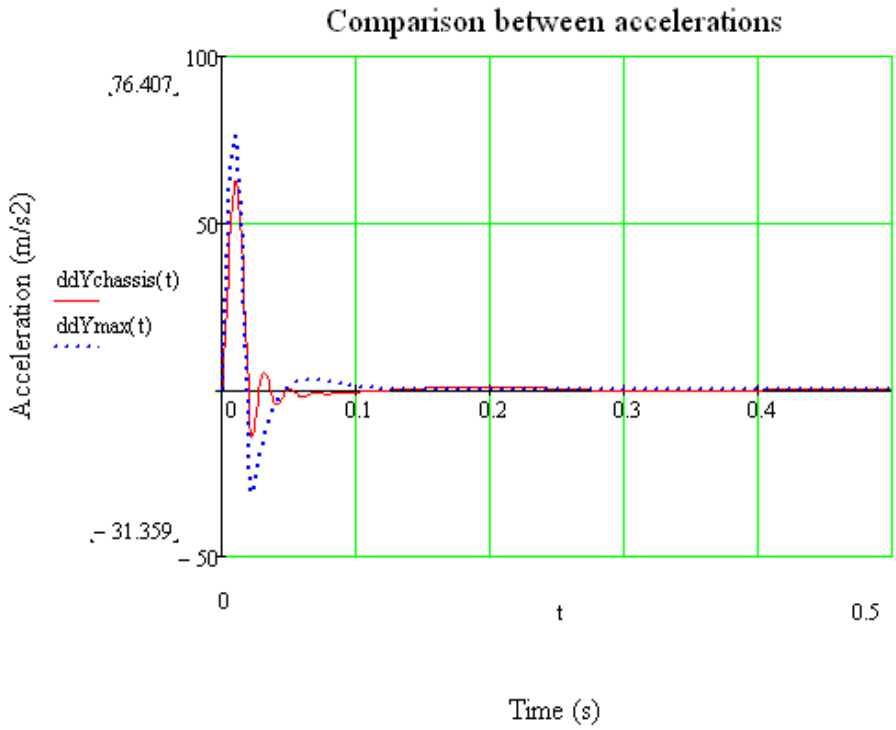

Figure 4.12. *Vertical acceleration with and without energy harvesting system.*

As is possible to observe from the Figure 4.12 the system with the energy harvesting system does not oscillate at all. This is traduced physically in a rough suspension that could alter the comfort of the passengers.

4.3. Third Model simulation

The third model simulation takes into account the dimension of the chassis and the difference between front and back wheels. The center of gravity is located at Lf from the front wheel and at Lb from the back wheel.

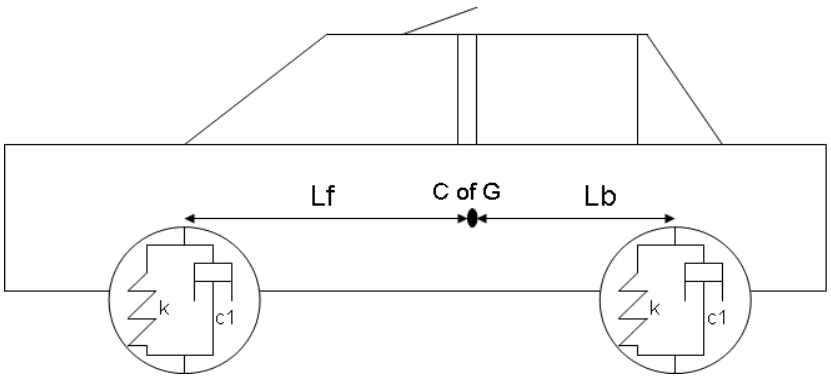

Figure 4.13. *Overview of the model design.*

This model has two degree of freedom which are the vertical displacement $Y_{chassis}$ and the twist $\theta_{chassis}$. The excitation source is the profile of the road $y_{road}(x)$.

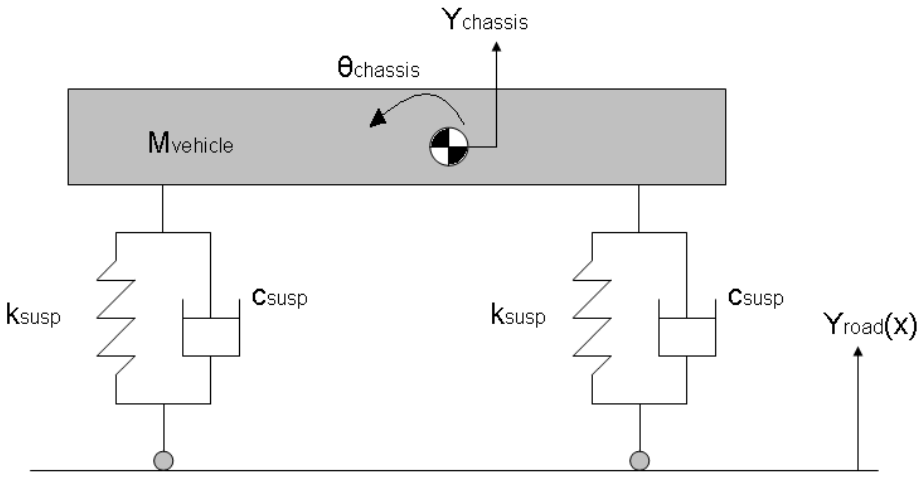

Figure 4.14. *Third model simulation.*

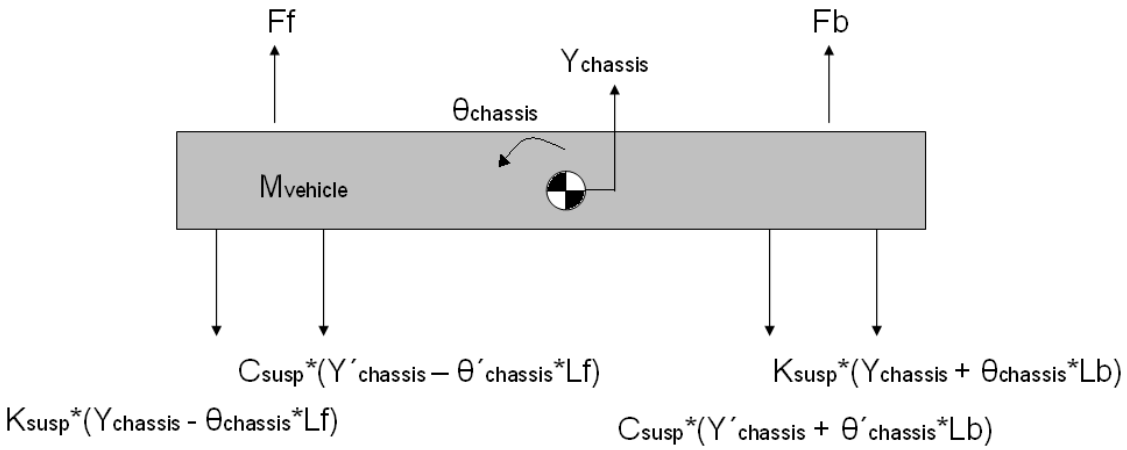

Figure 4.15. *Free body diagram of the third model simulation.*

The equations of motion for the system are based on the Figure 4.15

$$M_{vehicle}\ddot{Y}_{chassis} + 2c_{susp}\dot{Y}_{chassis} + (c_{susp}Lb - c_{susp}Lf)\dot{\theta}_{chassis} + 2k_{susp}Y_{chassis} + (k_{susp}Lb - k_{susp}Lf)\theta_{chassis} = F_f(t) + F_b(t)$$

$$J_{vehicle}\ddot{\theta}_{chassis} + (c_{susp}Lb - c_{susp}Lf)\dot{Y}_{chassis} + (c_{susp}Lb^2 + c_{susp}Lf^2)\dot{\theta}_{chassis} + (k_{susp}Lb - k_{susp}Lf)Y_{chassis} + \tag{4.12}$$

$$+ (c_{susp}Lb^2 + c_{susp}Lf^2)\theta_{chassis} = F_f(t)Lf + F_b(t)Lb$$

Rewriting these equations matrix form we can obtain the mass matrix, the damping matrix and the stiffness matrix.

$$[M] = \begin{bmatrix} M_{vehicle} & 0 \\ 0 & J_{vehicle} \end{bmatrix}$$

$$[C] = \begin{bmatrix} 2c_{susp} & c_{susp}Lb - c_{susp}Lf \\ c_{susp}Lb - c_{susp}Lf & c_{susp}Lb^2 + c_{susp}Lf^2 \end{bmatrix}$$

$$[K] = \begin{bmatrix} 2k_{susp} & k_{susp}Lb - k_{susp}Lf \\ k_{susp}Lb - k_{susp}Lf & k_{susp}Lb^2 + k_{susp}Lf^2 \end{bmatrix}$$

In this model the forces actuating into the wheels are different but it is possible to relate them with the total distance $Lf + Lb$.

$$F_f(t) = c_{susp}\dot{y}_{road}(t) + k_{susp}y_{road}(t)$$

$$F_b(t) = c_{susp}\dot{y}_{road}(t - \frac{Lf + Lb}{vel}) + k_{susp}y_{road}(t - \frac{Lf + Lb}{vel}) \tag{4.13}$$

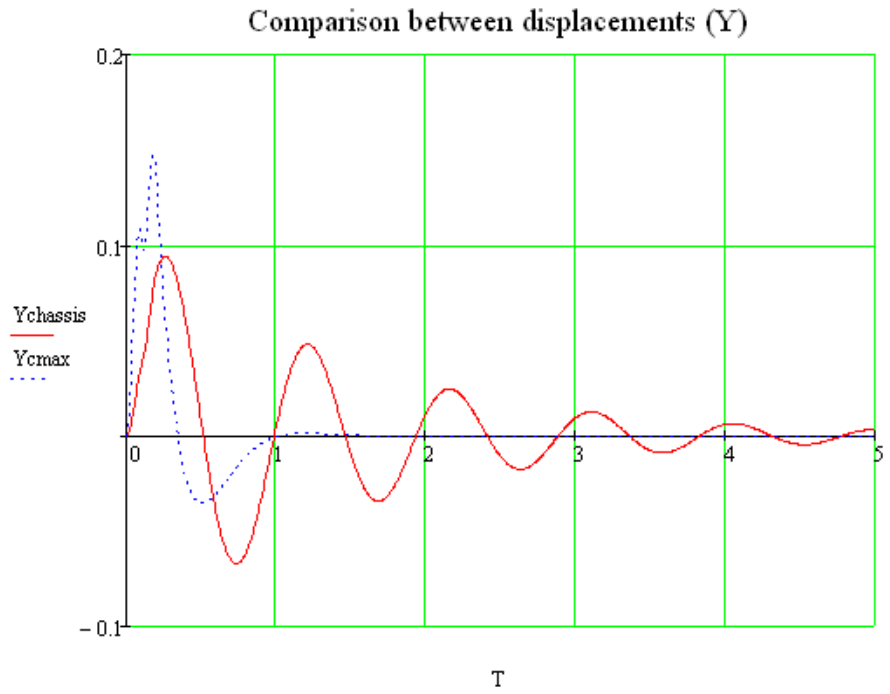

Figure 4.16. *Comparison between vertical displacements of chassis.*

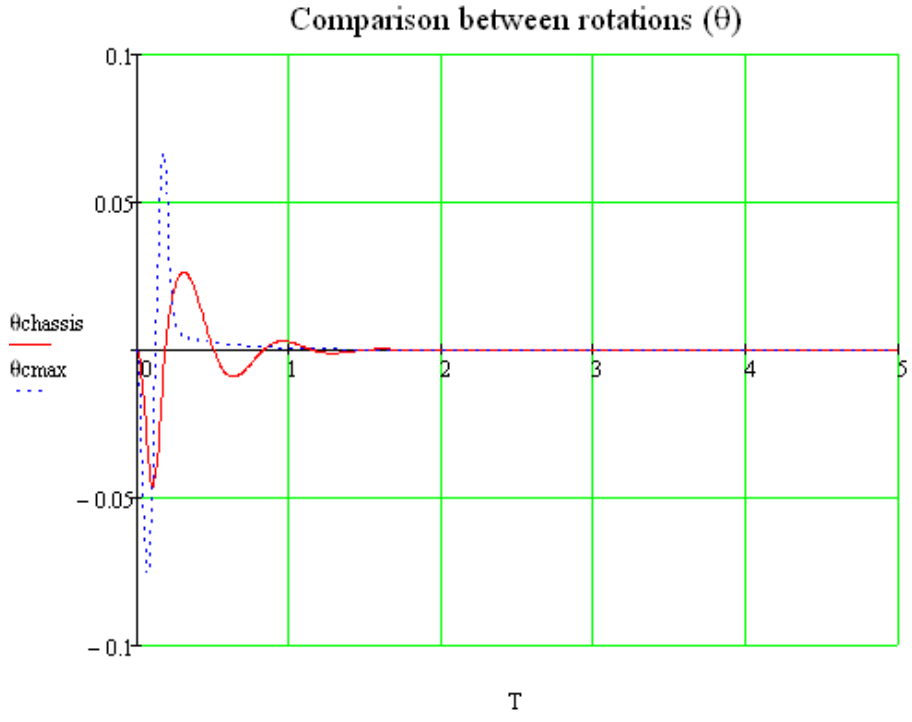

Figure 4.17. *Comparison between rotations of the chassis.*

The acceleration of the chassis is obtain using the equation 4.14

$$\ddot{Y}_{chassis}(t) = \frac{F_{force}(t) - c_{susp}\dot{Y}_{chassis}(t) - 2k_{susp}Y_{chassis}(t)}{M_{vehicle}} \tag{4.14}$$

If we compare the accelerations we can observe a huge difference between the one with the energy harvesting system and the one without.

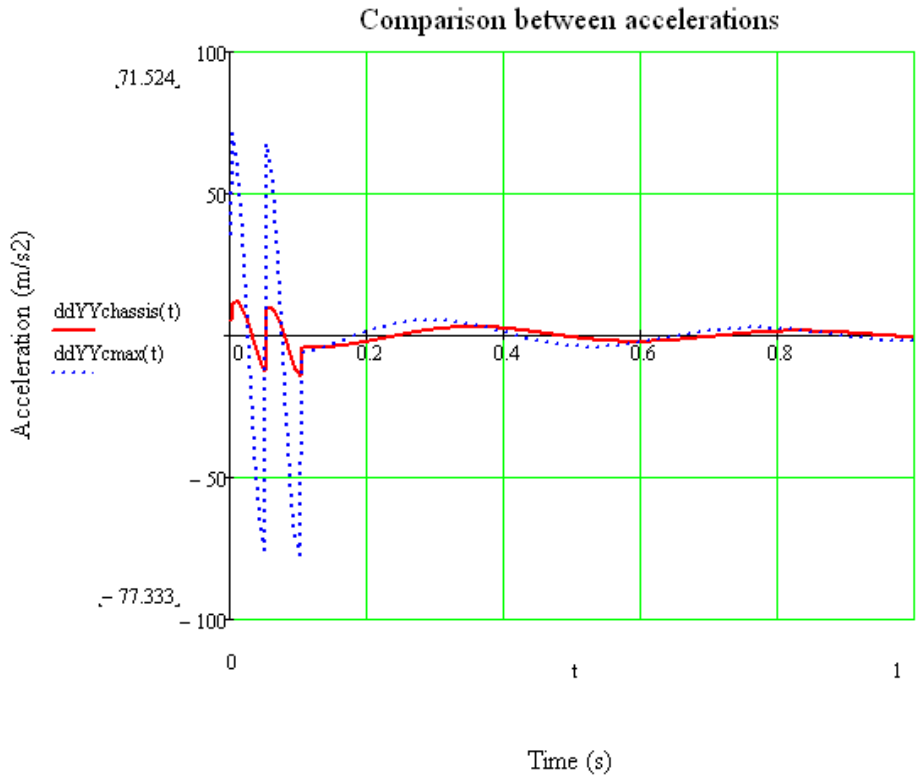

Figure 4.18. *Vertical acceleration with and without energy harvesting system.*

All the Mathcad code related to this model is shown in the appendix. Furthermore, an approximation in the amount of energy harvested is calculated.

4.4. Fourth Model Simulation

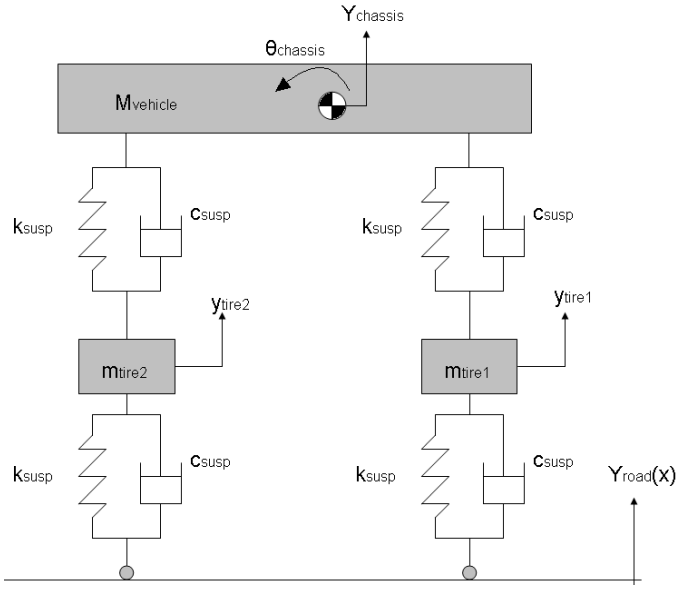

Figure 4.19 *Fourth model simulation.*

This is the most accurate model which consists in four degrees of freedom, the first one $Y_{chassis}$ is related to the vertical displacement of the chassis, the second $\theta_{chassis}$ is the rotation and the other two y_{tire1} y_{tire2} are the vertical displacement of each wheel.

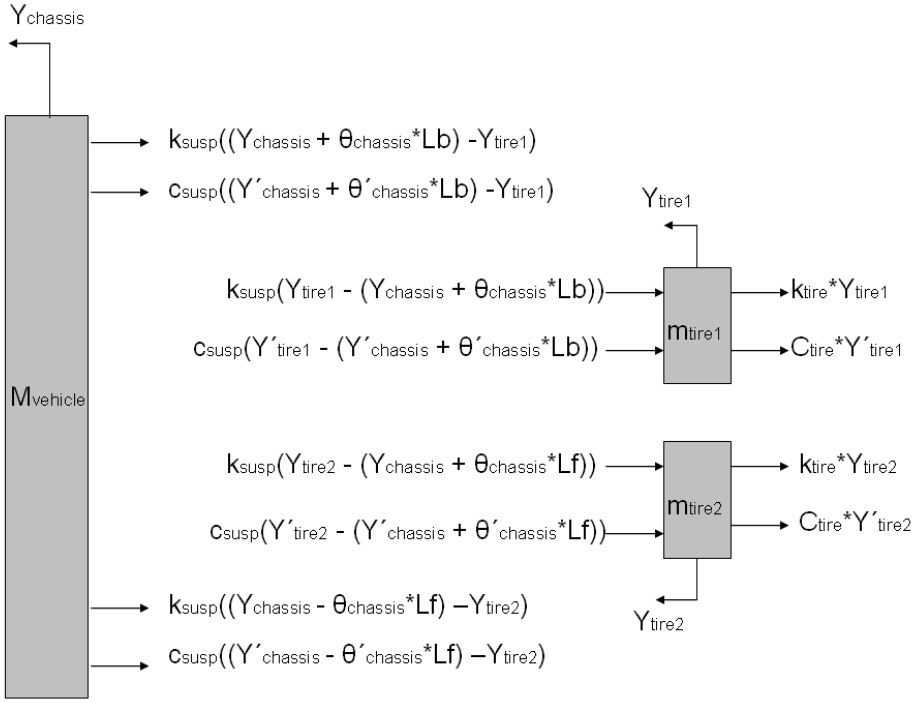

Figure 4.20. *Freebody diagram of the fourth model simulation.*

The equations of motion of the system using the free body diagram are shown in the equation 4.15 in a matrix form.

$$M\begin{bmatrix}\ddot{Y}_{chassis}\\ \ddot{\theta}_{chassis}\\ \ddot{y}_{tire1}\\ \ddot{y}_{tire2}\end{bmatrix}+C\begin{bmatrix}\dot{Y}_{chassis}\\ \dot{\theta}_{chassis}\\ \dot{y}_{tire1}\\ \dot{y}_{tire2}\end{bmatrix}+K\begin{bmatrix}Y_{chassis}\\ \theta_{chassis}\\ y_{tire1}\\ y_{tire2}\end{bmatrix}=\begin{bmatrix}0\\ 0\\ F_f\\ F_b\end{bmatrix} \tag{4.15}$$

$$M=\begin{bmatrix}M_{vehicle} & 0 & 0 & 0\\ 0 & J_{vehicle} & 0 & 0\\ 0 & 0 & m_{tire} & 0\\ 0 & 0 & 0 & m_{tire}\end{bmatrix}$$

$$C=\begin{bmatrix}2c_{susp} & c_{susp}(L_b-L_f) & -c_{susp} & -c_{susp}\\ c_{susp}(L_b-L_f) & c_{susp}(L_b^2+L_f^2) & -c_{susp}L_b & -c_{susp}L_f\\ -c_{susp} & -c_{susp}L_b & c_{susp}+c_{tire} & 0\\ -c_{susp} & -c_{susp}L_f & 0 & c_{susp}+c_{tire}\end{bmatrix}$$

$$K=\begin{bmatrix}2k_{susp} & k_{susp}(L_b-L_f) & -k_{susp} & -k_{susp}\\ k_{susp}(L_b-L_f) & k_{susp}(L_b^2+L_f^2) & -k_{susp}L_b & -k_{susp}L_f\\ -k_{susp} & -k_{susp}L_b & k_{susp}+k_{tire} & 0\\ -k_{susp} & -k_{susp}L_f & 0 & k_{susp}+k_{tire}\end{bmatrix}$$

In this model is necessary to use the modal coordinates in order to uncouple the equations and solve them independently. Then, the modal matrix is needed. To obtain the modal matrix we have to calculate the eigenvalues, eigenvectors and normalized them. The eigenvectors are normalized with the mass matrix.

$$genvals(K,M)=\begin{bmatrix}\lambda_1\\ \lambda_2\\ \lambda_3\\ \lambda_4\end{bmatrix}$$

$$genvecs(K,M)=\begin{bmatrix}\vec{\varphi}_1 & \vec{\varphi}_2 & \vec{\varphi}_3 & \vec{\varphi}_4\end{bmatrix}$$

$$\vec{\varphi}_{n1} = \frac{\vec{\varphi}_1}{\sqrt{\vec{\varphi}_1^{\,T} \cdot M \cdot \vec{\varphi}_1}}, \vec{\varphi}_{n2} = \frac{\vec{\varphi}_2}{\sqrt{\vec{\varphi}_2^{\,T} \cdot M \cdot \vec{\varphi}_2}}, \vec{\varphi}_{n3} = \frac{\vec{\varphi}_3}{\sqrt{\vec{\varphi}_3^{\,T} \cdot M \cdot \vec{\varphi}_3}}, \vec{\varphi}_{n4} = \frac{\vec{\varphi}_4}{\sqrt{\vec{\varphi}_4^{\,T} \cdot M \cdot \vec{\varphi}_4}}$$

$$\Omega = \begin{bmatrix} \vec{\varphi}_{n1} & \vec{\varphi}_{n2} & \vec{\varphi}_{n3} & \vec{\varphi}_{n4} \end{bmatrix}$$

The damping matrix is a linear combination of the mass and stiffness matrices.

$$\eta = \Omega X$$
$$\dot{\eta} = \Omega \dot{X}$$
$$\ddot{\eta} = \Omega \ddot{X}$$
$$Q = \Omega^T \begin{bmatrix} 0 \\ 0 \\ F_f(t) \\ F_b(t) \end{bmatrix}$$

$$\ddot{\eta} + (\alpha I + \beta \Gamma)\dot{\eta} + \Gamma \eta = Q$$

$$M_{modal} = \begin{bmatrix} 1 & 0 & 0 & 0 \\ 0 & 1 & 0 & 0 \\ 0 & 0 & 1 & 0 \\ 0 & 0 & 0 & 1 \end{bmatrix}$$

$$\Gamma = K_{modal} = \Omega^T \cdot K \cdot \Omega = \begin{bmatrix} \lambda_1 & 0 & 0 & 0 \\ 0 & \lambda_2 & 0 & 0 \\ 0 & 0 & \lambda_3 & 0 \\ 0 & 0 & 0 & \lambda_4 \end{bmatrix}$$

$$C_{modal} = \alpha I + \beta \Gamma = \frac{c_{susp}}{k_{susp}} \Gamma = \begin{bmatrix} 2.496 & 0 & 0 & 0 \\ 0 & 5.977 & 0 & 0 \\ 0 & 0 & 292.259 & 0 \\ 0 & 0 & 0 & 292.692 \end{bmatrix}$$

$$Q(t) = \Omega \begin{bmatrix} 0 \\ 0 \\ F_f(t) \\ F_b(t) \end{bmatrix}$$

The Runge Kutta method is applied to the modal coordinates.

$$Origin = 1$$
$$t_0 = 0$$
$$t_{\max} = 5$$

$$Invalues = \begin{bmatrix} 0 \\ 0 \\ 0 \\ 0 \end{bmatrix}$$

$$D_1(t,y) = \begin{bmatrix} y_3 \\ y_4 \\ Q(t)_1 - C_{modal1,1} y_3 - \Gamma_{1,1} y_1 \\ Q(t)_2 - C_{modal1,1} y_4 - \Gamma_{1,1} y_2 \end{bmatrix}$$

$$S_1 = rkfixed(Invalues, t_0, t_{\max}, 500, D_1)$$
$$T1 = S_1^{\langle 1 \rangle}$$
$$\eta_y = S_1^{\langle 2 \rangle}$$
$$\eta_\theta = S_1^{\langle 3 \rangle}$$
$$d\eta_y = S_1^{\langle 4 \rangle}$$
$$d\eta_\theta = S_1^{\langle 5 \rangle}$$

$$D_2(t,y) = \begin{bmatrix} y_3 \\ y_4 \\ Q(t)_3 - C_{modal3,3} y_3 - \Gamma_{3,3} y_1 \\ Q(t)_4 - C_{modal4,4} y_3 - \Gamma_{4,4} y_2 \end{bmatrix}$$

$$T1 = S_2^{\langle 1 \rangle}$$
$$\eta_{ytire1} = S_2^{\langle 2 \rangle}$$
$$\eta_{ytire2} = S_2^{\langle 3 \rangle}$$
$$d\eta_{ytire1} = S_2^{\langle 4 \rangle}$$
$$d\eta_{ytire2} = S_2^{\langle 5 \rangle}$$

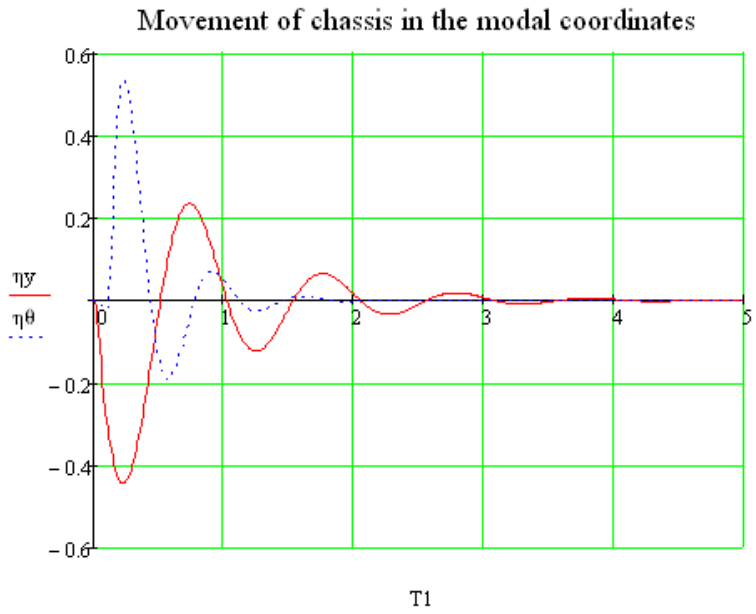

Figure 4.21. *Movement of chassis in the modal coordinates.*

In the real coordinates

$$X(t) = \Omega \begin{bmatrix} \eta_y \\ \eta_\theta \\ \eta_{ytire1} \\ \eta_{ytire2} \end{bmatrix}$$

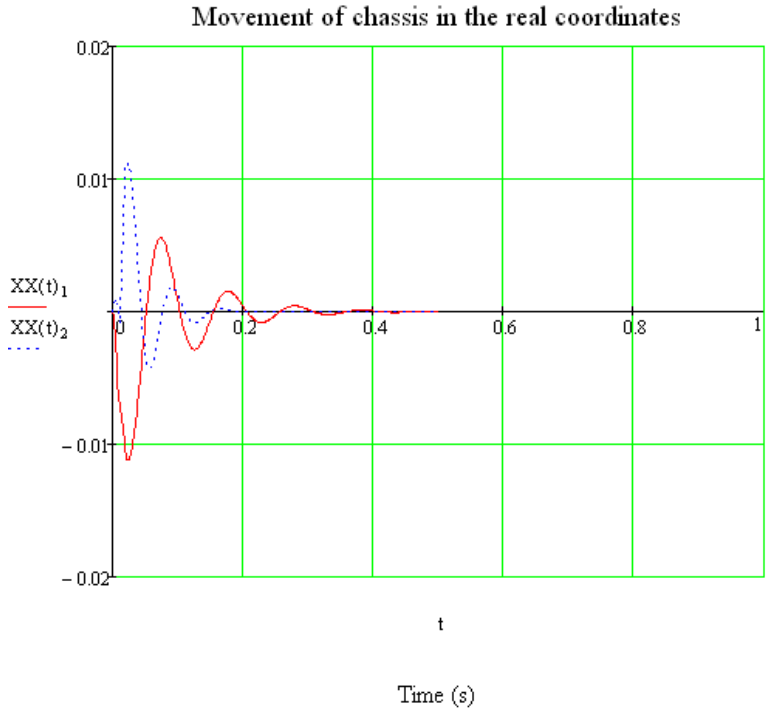

Figure 4.22. *Movement of the chassis in the real coordinates* $Y_{chassis}$ $\theta_{chassis}$.

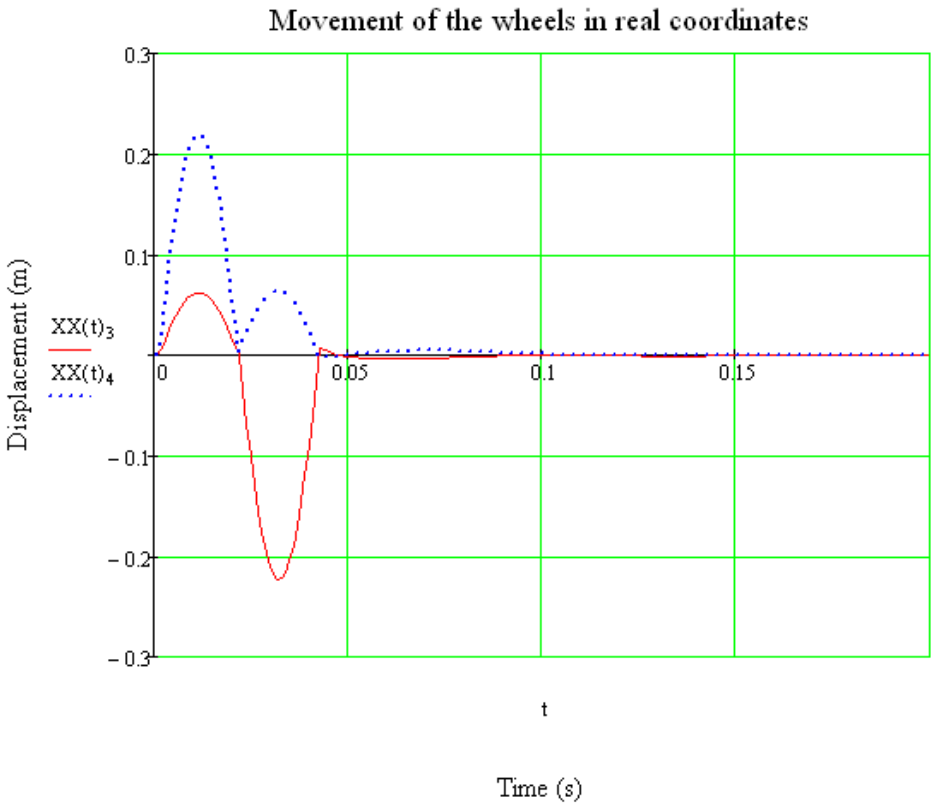

Figure 4.23. *Movement of the wheels in the real coordinates.*

Accelerations in the modal coordinates.

$$\ddot{X}_{m1}(t) = Q(t)_1 - C_{modal_{1,1}} d\eta_y - \Gamma_{1,1}\eta_y$$
$$\ddot{X}_{m2}(t) = Q(t)_2 - C_{modal_{2,2}} d\eta_\theta - \Gamma_{2,2}\eta_\theta$$
$$\ddot{X}_{m3}(t) = Q(t)_3 - C_{modal_{3,3}} d\eta_{ytire1} - \Gamma_{1,1}\eta_{ytire1}$$
$$\ddot{X}_{m4}(t) = Q(t)_4 - C_{modal_{4,4}} d\eta_{ytire2} - \Gamma_{1,1}\eta_{ytire2}$$

Transforming to the real coordinates using the modal matrix.

$$\ddot{X}(t) = \Omega \begin{bmatrix} \ddot{X}_{m1}(t) \\ \ddot{X}_{m2}(t) \\ \ddot{X}_{m3}(t) \\ \ddot{X}_{m4}(t) \end{bmatrix}$$

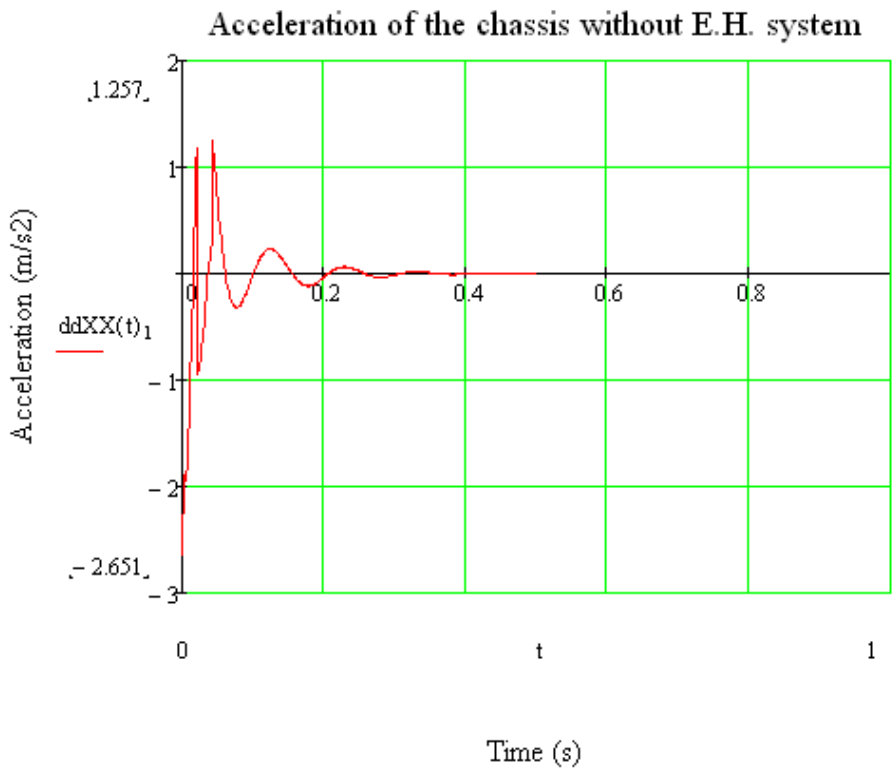

Figure 4.24. *Vertical acceleration of the chassis in real coordinates.*

Comparison when we introduce the energy harvesting system.

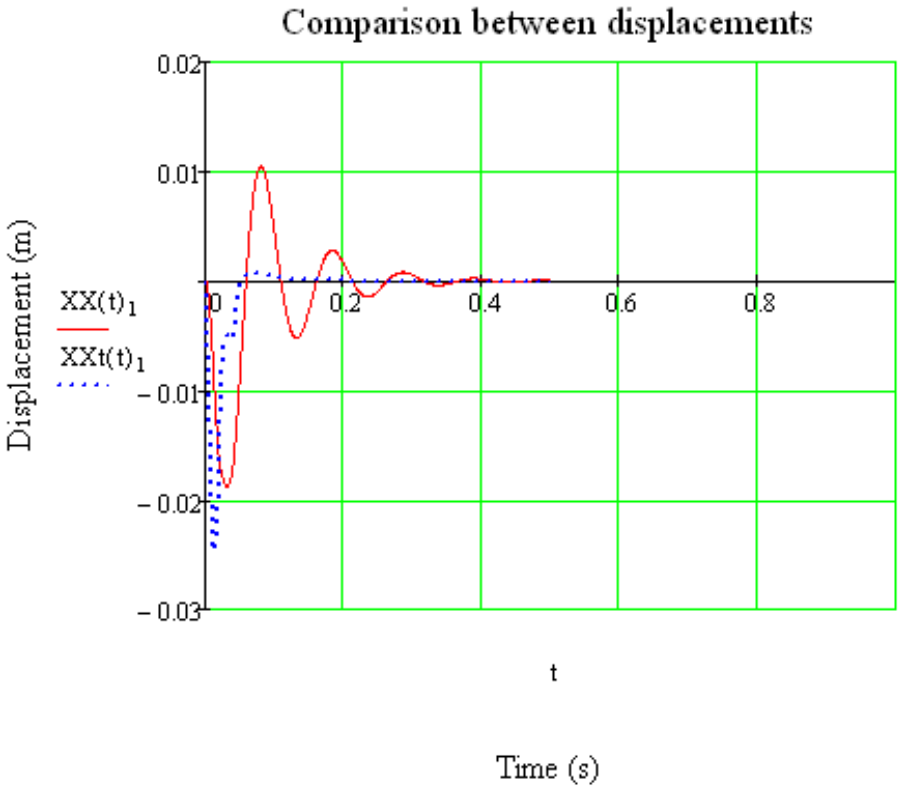

Figure 4.25. *Displacements with and without energy harvesting system.*

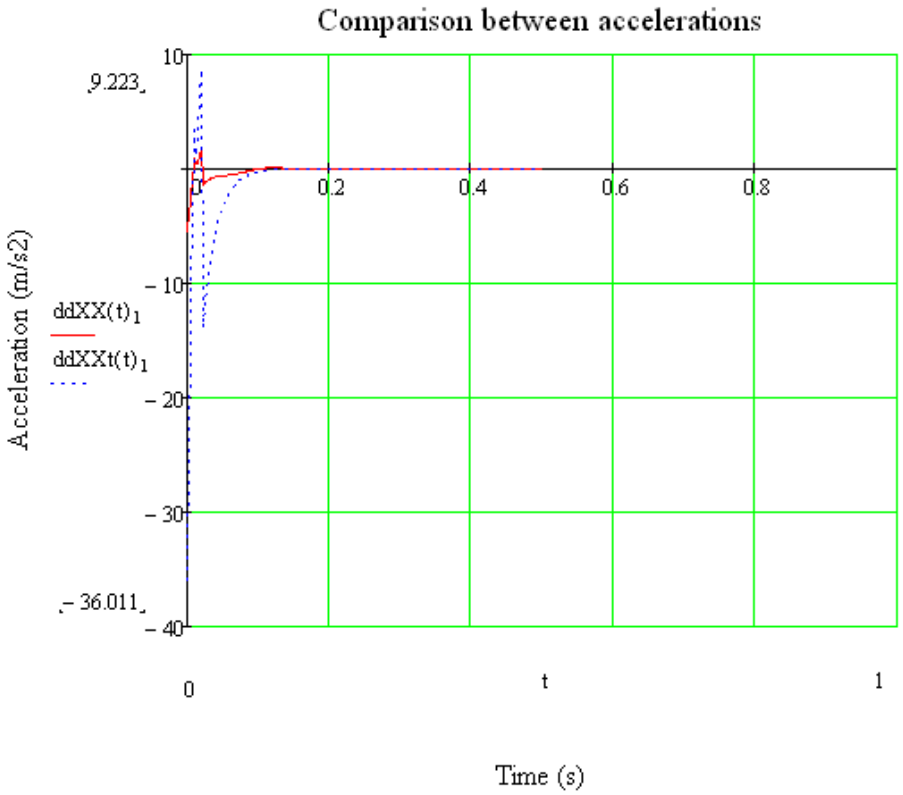

Figure 4.26. *Comparison between accelerations velocity 30,54m/s.*

It is also interesting to observe the changes when the velocity of the vehicle change.

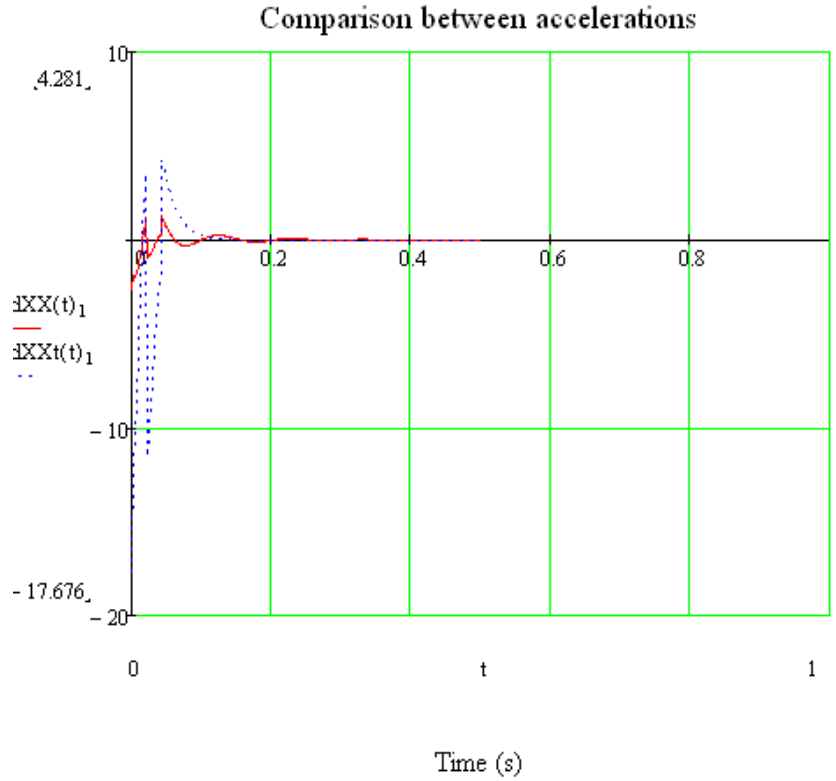

Figure 4.27. *Comparison of accelerations for velocity 15m/s.*

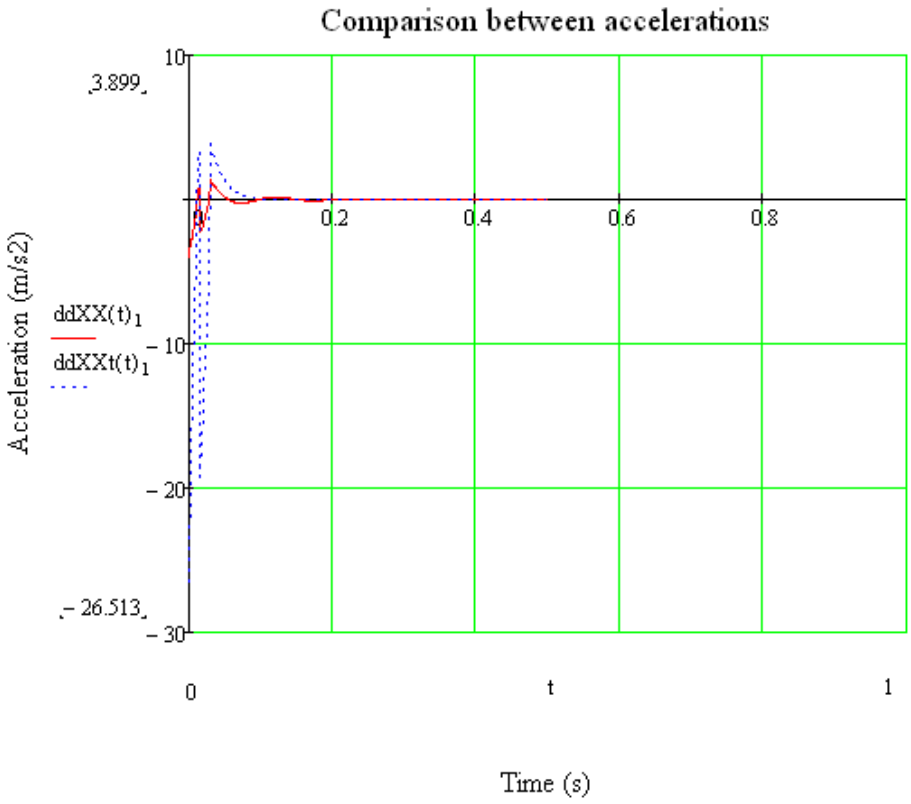

Figure 4.28. *Comparison of accelerations for velocity 22,5m/s.*

It is possible to observe in the last three figures that a reduction in the speed of the vehicle is traduced in a reduction in the maximum peak of the vertical acceleration in this case the negative one. However, the positive one is bigger when the vehicle's velocity is $15m/s$ than when the velocity is $22{,}5m/s$. This is an important fact to take into account.

In order to calculate the amount of energy harvested by this system, the equation 4.8 must be modified due to both wheels contribute.

$$W_{tire1} = \int_0^{t_1} c_{t\max} \cdot (\dot{Y}_{chassis}(t) - \dot{y}_{road}(t))^2 \, dt$$

$$W_{tire2} = \int_0^{t_2} c_{t\max} \cdot (\dot{Y}_{chassis}(t) - \dot{y}_{road}(t))^2 \, dt$$

$$W_{total} = W_{tire1} + W_{tire2} \tag{4.16}$$

where the times t_1 and t_2 are related by

$$t_2 = t_1 - \frac{Lb + Lf}{v}$$

It is also interesting to observe the changes for different sizes of bumps. It is possible to put the bump as a function of their length *L* and height *A*. Now we will focus only in the vehicle with the energy harvesting system.

$$M_{vehicle} = 2500kg$$
$$J_{vehicle} = 1860kg \cdot m$$
$$m_{tire} = 85kg$$

$$y_{road}(x) = \frac{A}{2}\left(1+\cos\left(2\pi\left(\frac{x}{L}-\frac{1}{2}\right)\right)\right)$$

$$y_{road}(t) = \frac{A}{2}\left(1+\cos\left(2\pi\left(\frac{vt}{L}-\frac{1}{2}\right)\right)\right)$$

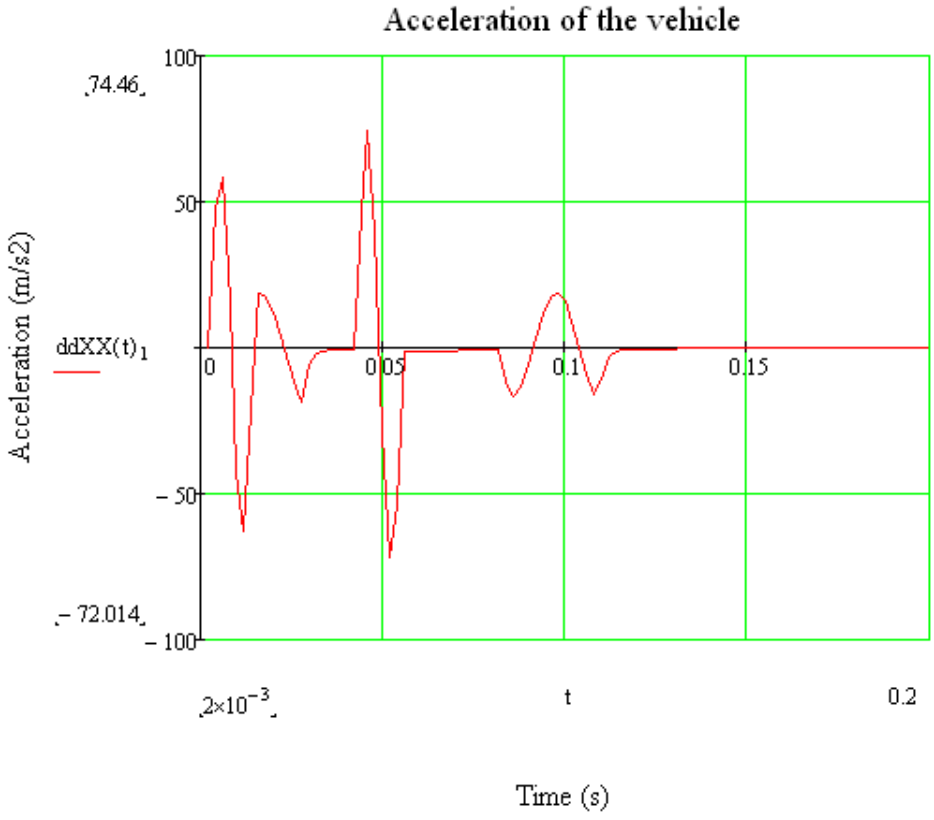

Figure 4.29. *Acceleration for $A = 0{,}5m$ $L = 1m$ and velocity 30,54m/s without energy harvesting system.*

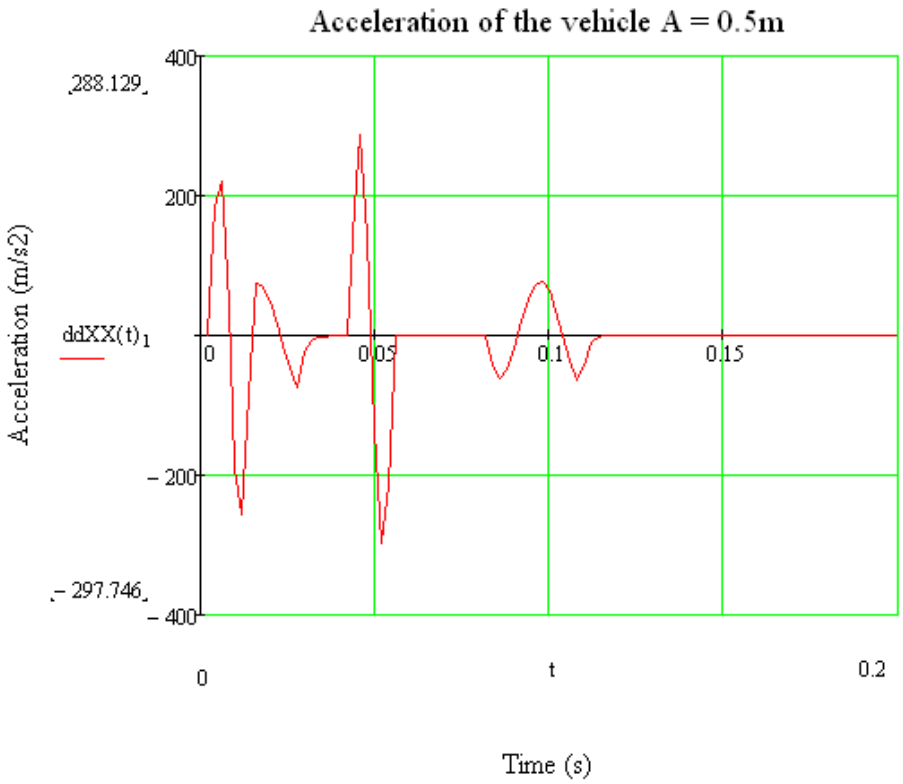

Figure 4.30. *Acceleration for* $A = 0.5m$ $L = 1m$ *and velocity 30,54m/s with energy harvesting system.*

Changing the shape of the bump

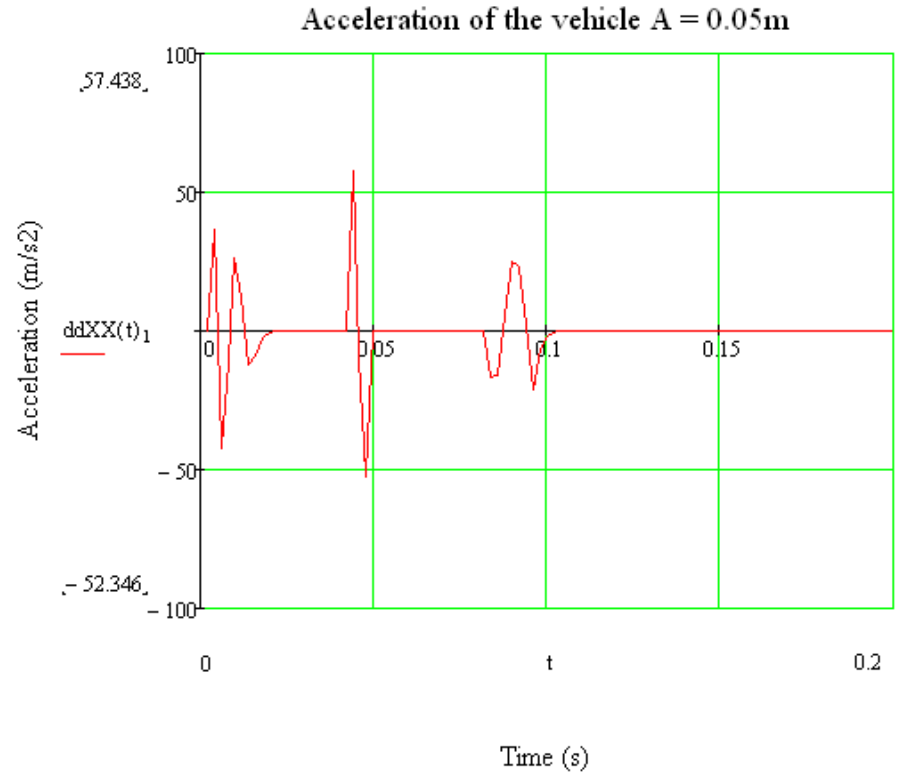

Figure 4.31. *Acceleration for* $A = 0.05m$ $L = 0.5m$ *and velocity 30,54m/s with energy harvesting system.*

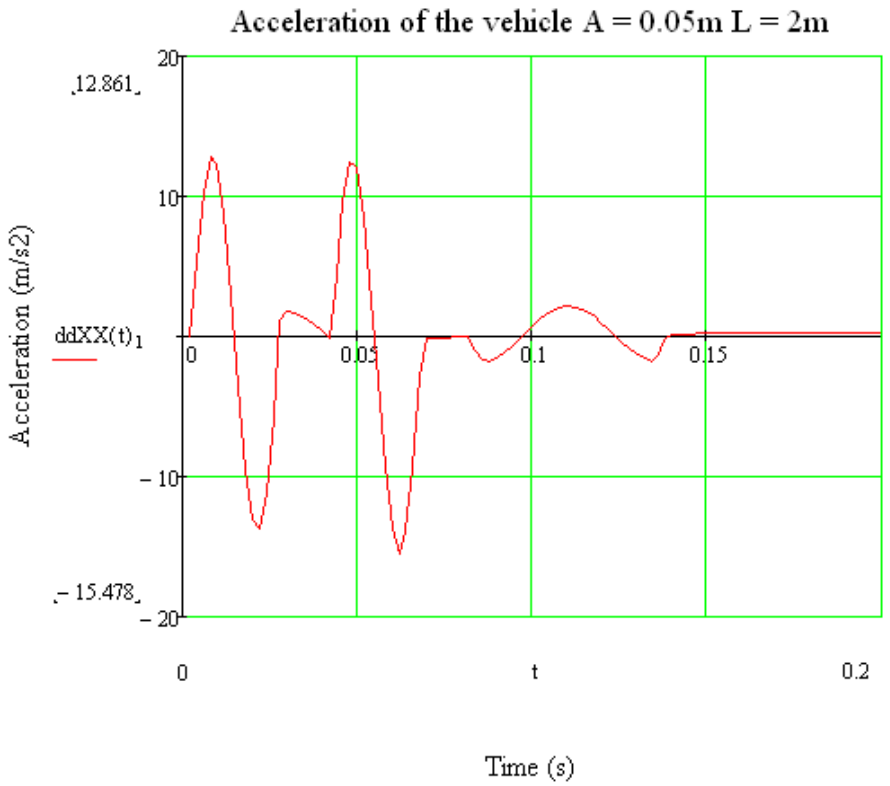

Figure 4.32. *Acceleration for* $A = 0.05m$ $L = 2m$ *and velocity 30,54m/s with energy harvesting system.*

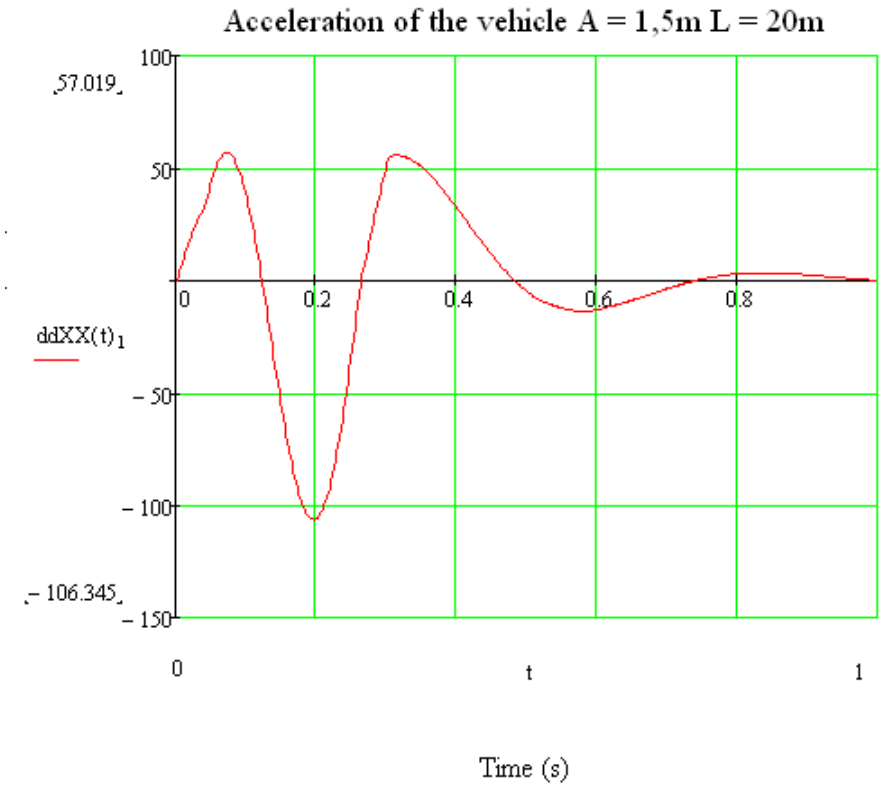

Figure 4.33. *Acceleration for* $A = 1.5m$ $L = 20m$ *and velocity 30,54m/s with energy harvesting system.*

Changing the velocity of the vehicle from $30{,}54 m/s$ to $15 m/s$

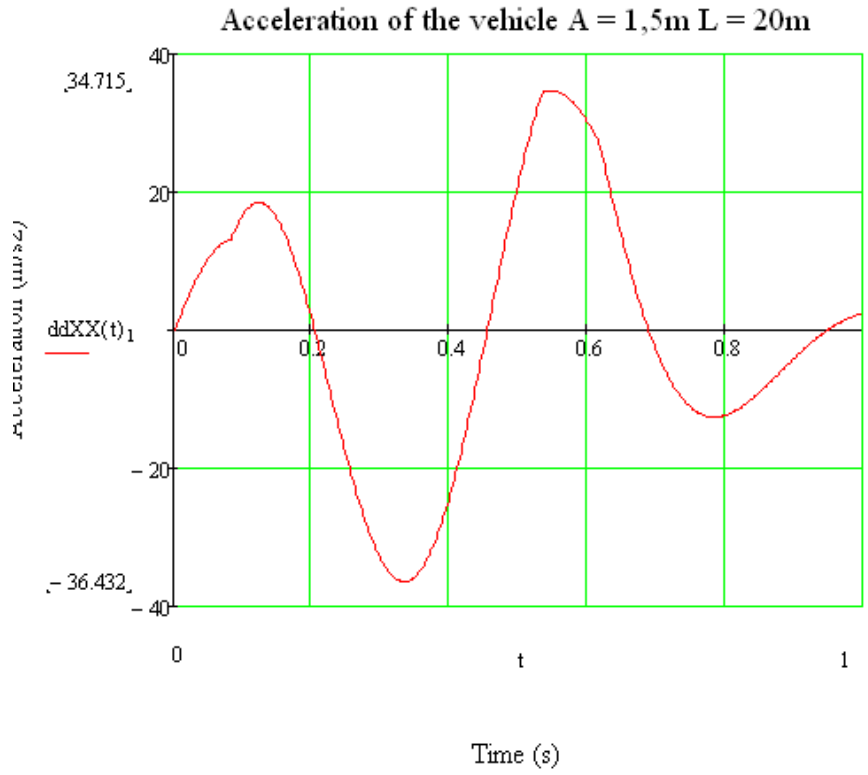

Figure 4.34. *Acceleration for $A = 1.5m$ $L = 20m$ and velocity 15m/s with energy harvesting system.*

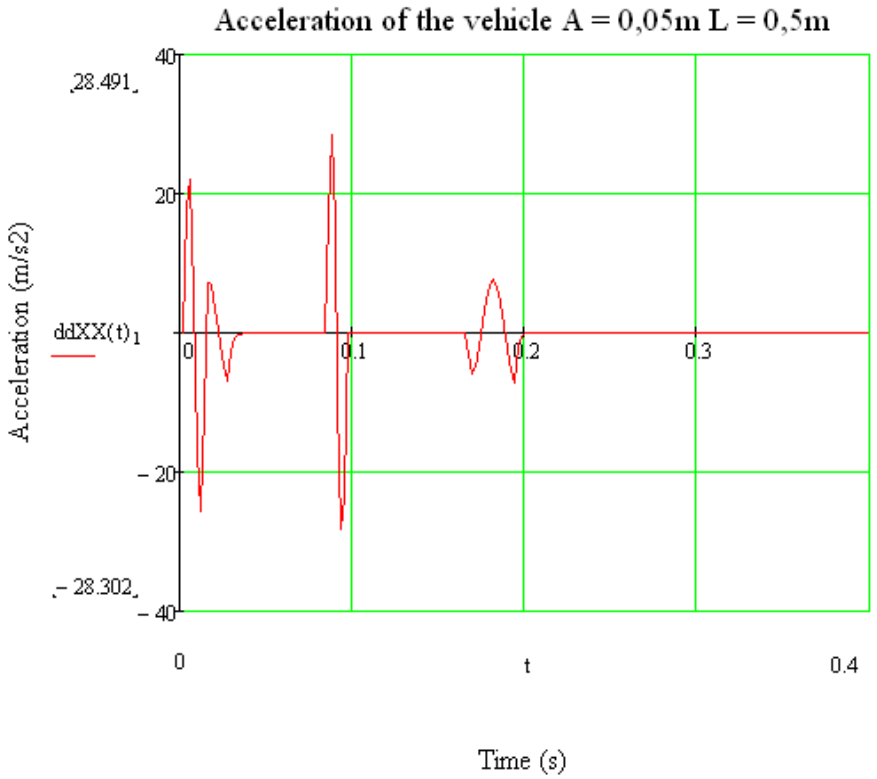

Figure 4.35. *Acceleration for $A = 0.05m$ $L = 0.5m$ and velocity 15m/s with energy harvesting system.*

Changing the mass of the vehicle from $M_{vehicle} = 2500kg$ to $M_{vehicle} = 1800kg$:

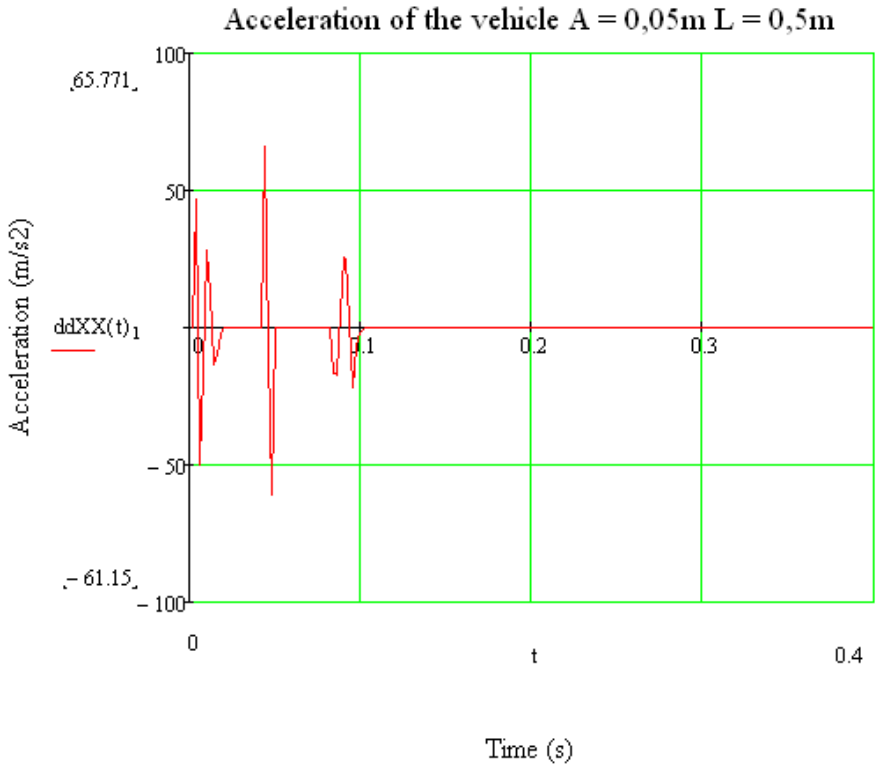

Figure 4.36. Acceleration for $A = 0.05m$ $L = 0{,}5m$ and velocity 30,54*m/s* with energy harvesting system. $M_{vehicle} = 1800kg$ $J_{vehicle} = 1810kg \cdot m$ $m_{tire} = 75kg$.

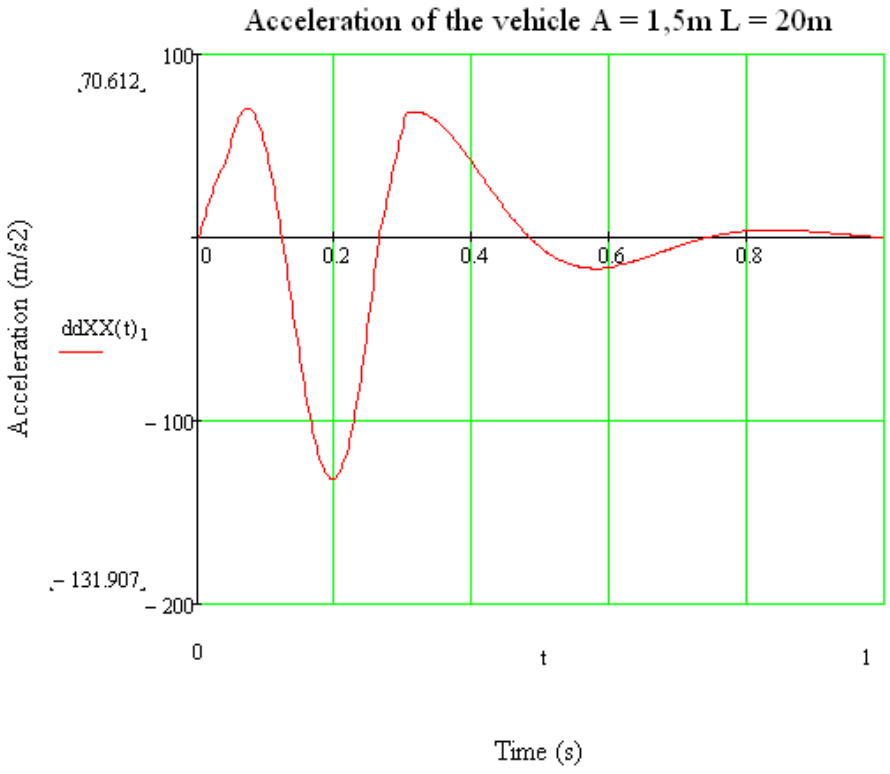

Figure 4.37. *Acceleration for* $A = 1.5m$ $L = 20m$ *and velocity 30,54m/s with energy harvesting system.* $M_{vehicle} = 1800kg$ $J_{vehicle} = 1810kg \cdot m$ $m_{tire} = 75kg$.

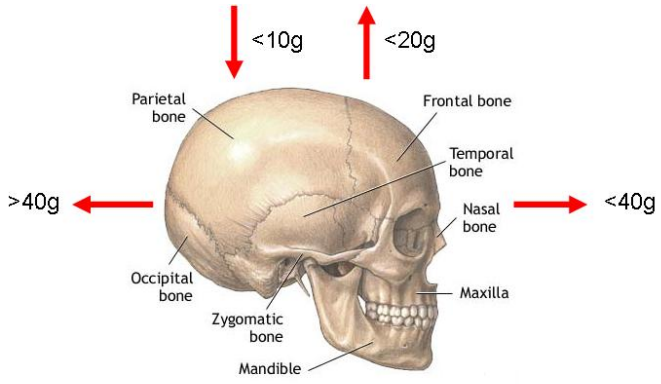

Figure 4.38. *Limits of the instant acceleration for the human being.*

The Figure 4.38 shows the acceleration limits in the skull for the human being. The thoracic cage could support 60g but the vertebral spine only around 20g. The limit values of the Figure 4.38 are for instant accelerations. Therefore, if there are continuous bumps in the road the accelerations become prolonged and the limits will decrease so that is why it will be interesting to reduce the damping of the system from $C_{damping} = 16980 Ns/m$ to $C_{damping} = 10000 Ns/m$. With this reduction the acceleration of the system is going to be $\cong 3g$ instead of $\cong 6g$. The main problem of this reduction is that the amount of energy harvesting decreases.

Reducing the damping coefficient:

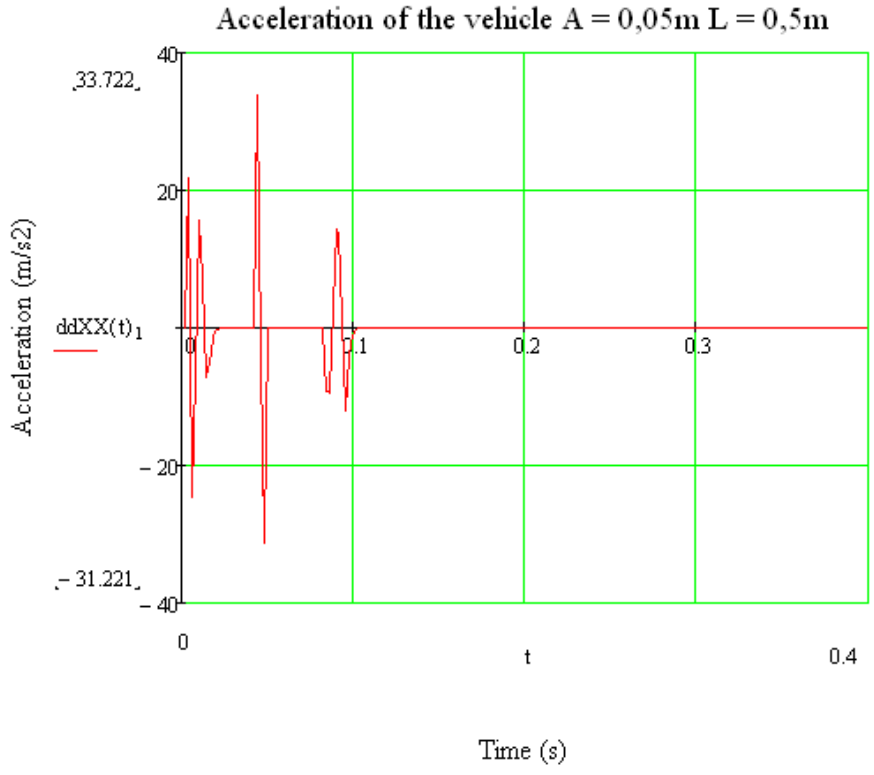

Figure 4.39. *Acceleration for* $A = 0.05m$ $L = 0.5m$ *and velocity 30,54m/s with energy harvesting system.* $C_{damping} = 10 \times 10^4 Ns/m$.

4.5. Results and Discussion

In the first model the main aim is to observe the consequences when we introduce an energy harvesting system into a simple model passing through a simple bump. The energy harvesting system is introduced inside the damper and this is reflected in the model as an increase in the damping factor. The increase in the damping factor is limited when the system gets over damped. According to this all the calculations in the rest of the simulations are for the system with the maximum damping factor. The Figure 4.8 shows an important change in the vertical acceleration of the chassis as a result of the energy harvesting system. The values of acceleration the chassis supporting is around $6.6g$, but in less than 0.2sec. On account of the acceleration lasting less than 1sec the acceleration is considered instant so there is not harmful for the human being.

In the second model simulation the tire is considered as a separately mass, this gives to the model more accuracy and the peak of the acceleration with this model reaches $7g$ as is shown in the Figure 4.12. In the third model simulation there is a comparison between displacements and rotations in Figure 16 and Figure 17 respectively. Both Figures shows how the system with the energy harvesting system does not oscillate at all. Concerning the vertical acceleration of the chassis the maximum values obtained are similar to the previous models. In the fourth model it is important to remark that changing the velocity of the vehicle helps reducing the maximum peak of the acceleration but could increase another peak as is shown in the Figure 4.26, Figure 4.27, and Figure 4.28.

In the real life the most problematic bumps are the ones shown is Figure 4.31 and Figure 4.33. The first one consists on small amplitude and length, represents some imperfection on the road caused most likely by the trucks. The maximum vertical acceleration of the chassis is 6g and could be harmful for the driver at some point if the road contained a group of them. Another realistic bump is the one which appears when a road passes through a hill, the road then goes up 1.5 meters in 20 meters long, causing an acceleration of the chassis of 6g. Again, the reiteration of any of these bumps could change the character of the acceleration from instant into prolonged. As a result of that the limits of the Figure 4.37 will not be valid. New limits more restrictive should be used so 6g could be harmful for the human being.

The modification of the parameters such as velocity and mass of the vehicle show which type of vehicle is going to be more vulnerable. The reduction in velocity and the increase in mass reduce the peaks in the acceleration response so this means that trucks are going to be able to overcome better this problem. Finally, in order to reduce the 6g of vertical acceleration in the chassis with the bump $A = 0.05m$ $L = 0.5m$ a reduction in the damping coefficient is needed, the vertical acceleration of the chassis reduces to 3g. Now the system in complete safe no matter which bumps goes through.

To conclude, even though the system is able to harvest the maximum amount of energy the limits of the human being against the vertical accelerations force to reduce the amount of energy harvesting with the purpose of the system been safe.

5. CONCLUSIONS

The objective of this Masters Thesis was to harvest energy from a vehicle suspension in order to decrease the consumption of fuel in the vehicle. The introduction of the energy harvesting system results in an increase of the system damping. Both the amount of energy harvest in the suspension and the ergonomics of the driver depend on the system damper. According to this it was important to make a balance between the ergonomics of the passenger and the amount of energy harvested.

There are diverse ways to harvest energy with different systems and between all of them the hydraulic system was the best one in terms of efficiency which was our purpose for the vehicle. The implementation of the energy harvesting system is traduced physically in a special damper that is able to work as a damper as well as recovering energy at the same time through a hydraulic piston and theoretically in an increase on the system damping. This increase is limited by the system over-damped, but the possibility of being harmful for the human being settles a more restrictive limit. The results of the model with the energy harvesting system increase the acceleration in the chassis of the vehicle. The maximum values of acceleration take place in a very short time, namely less than 0.2seconds which are considered as instant. On the other hand, if the acceleration is more than two seconds then it is considered to be prolonged. Since human tissues are viscoelastic, which means that the material properties vary with strain rate, the response of the body to acceleration varies with duration exposure. During impact accelerations, acceleration tolerance increases as the exposure duration decreases.

To sum up, the introduction of the energy harvesting system in vehicle suspension is successful in general terms, but could be harmful for the human being in a specific situation depending on the profile of the road. The possibility to the appearance of consecutive bumps could increase the duration of the maximum value of the acceleration and therefore, instead of considering it an impact, it will turn into prolonged acceleration. As is shown in the simulation, the reduction in the velocity of the vehicle decreases the maximum value of acceleration but prolongs it in time. Moreover, the mass of the vehicle play an important role because if the mass increases then the damping could also be increased without over-passing any of the limits.

The future investigations will focus on how a vehicle could harvest the maximum amount of energy in any kind of terrain without exceeding the physical human limits. Potential improvements in the hydraulic system could result in an increase of the efficiency. This increase on the efficiency will allow the system to reduce the damping necessary to harvest the maximum energy. Due to the success in the vehicles industry recent studies have been made for harvesting energy in industrial machines in order to save fuel.

REFERENCES

Ahmad, M. E. 2005. Energy Harvesting Using a Cheap Easy-to-Fabricate FM Rectenna. Alexandria University Egypt, Marine Enginnering Department.

Automotive Research Center. Supplemental Vehicle Power through Innovative Energy Harvesting. http://arc.engin.umich.edu/arc/research/ta1/T1_13.htm. Accessed 7 of October of 2009.

Bart, L., Gysen, J., Johannes, J., Paulides, H., Jeroen, L., Janssen, G. & Lomonova, E. A. 2008. Active Electromagnetic Suspension System for Improved Vehicle Dynamics. Eindhoven University of Technology. September, 2008.

Beeby, S. P., Tudor, M. J. & White, N. M. 2006. Energy Harvesting Vibration Sources For Microsystems Applications. Review article. School of Electronics and Computer Science, University of Southampton S017 1BJ, UK.

Boeing Spectrolab. Photovoltaics Space Products. http://www.spectrolab.com/space.htm. Accessed 15 November 2009.

Bolton, W. 2003. Mechatronics, Electronic control systems in mechanical and electrical engineering. Third edition. Edinburgh Gate.

Bose Suspension System. Engineering a smother and more stable ride. http://www.bose.com/controller?url=/automotive/bose_suspension/index.jsp. Accessed 16 of January of 2010.

Earl Logan, JR. 1981. Turbomachinery, basic theory and applications. Department Of Mechanical Engineering. Arizona State University. Tempe, Arizona.

Esteban, G., Güemez B. & Peña, A. 2006. Mecánica de Fluidos. Second Volume. Department of Nuclear Engineering and fluid Mechanics. Escuela Técnica Superior de Ingenieros. Bilbao, Spain.

Guillot, Francois M., Beckham, Haskell W., Leisen, J. 2007. Piezoelectric Fabrics for Energy Harvesting. National Textile Center, Annual report. November, 2007.

Gupta, A., Jendrzejczyk, J.A., Mulcahy, T.M. & Hull J.R. 2007. Design of electromagnetic shock absorbers. Northern Illinois University. 22 of May, 2007.

Levant Power Corporation. http://www.levantpower.com/. Accessed 1 of November of 2009.

Lewis, F.L. 2004. Wireless Sensor Networks. Automation and Robotics Research Institute. The University of Texas at Arlington. New York.

Milliken W. F. & Milliken D. L. 1995. Race Car Vehicle Dynamics. First edition, 1995.

Mitcheson P. D. & Yeatman E.M. 2009. Energy Harvesting for Pervasive Computing. Imperial college of London. 2009.

Murugavel Raju. 2008. Ultra-low-power Meets Energy Harvesting. White paper, MCU strategic marketing. Texas instrument incorporated. November, 2008.

Ostaffe, H. 2009. RF Energy Harvesting Enables Wireless Sensor Networks. Sensors Mag. 13 October.

Park, G., Farrar, C. R., Todd, M. D., Hodgkiss, W & Rosing, T. 2007. Energy Harvesting for Structural Health Monitoring Sensor Networks. February, 2007.

Pickelmann, Dr. Lutz GmbH. 2003. Piezomechanik introduction. September 2003, Munich.

Pickelmann, Dr. Lutz GmbH. 2004. Piezomechanik piezo-mechanical and electrostrictive stack and ring actuators. January 2004, Munich.

Priya, S. & Inman, D. 2009. Energy Harvesting Technologies. Springer Science and Business Media.

Sodano, H. & Inman, D. 2005. Comparison of Piezoelectric Energy Harvesting Devices for Recharging Batteries. Journal of Intelligent Material System and Structures. Center for Intelligent Material Systems and Structures.

Swee L. Kok, Neil M. White and Nick R. Harris. 2009. Free-Standing Thick-Film Piezoelectric Multimorph Cantilevers for energy harvesting. University of Southampton. July, 2009.

Xie, J., Mane, P.P., Green, C.W., Mossi, K.M., Leang, Kam K. 2008. Energy Harvesting By Pyroelectric Effect Using PZT. ASME Conference on Smart Materials Structures and Intelligent Systems. October 28-30, 2008, Ellicott City, Maryland, USA.

APPENDIX

The appendix shows the Mathcad code of the third model simulation. Firstly the vehicle parameters are defined. Secondly the equations of motion are calculated and finally the simulation part is carried out from a particular excitation source.

Mvehicle := 1800

ksusp := 40000

Jvehicle := 1860

Lf := 1.7 Distance from the centre of gravity to the front wheel

Lb := 1.4 Distance from the centre of gravity to the back wheel

$csusp := \zeta susp \cdot \sqrt{ksusp \cdot Mvehicle} = 2.546 \times 10^3$

cmaxh := 14430 Max Added damping as a result of the harvesting system

Jvehicle := 1860

$ctmax := csusp + cmaxh = 1.698 \times 10^4$

ktire := 350000

mtire := 85

$$Mm := \begin{pmatrix} Mvehicle & 0 \\ 0 & Jvehicle \end{pmatrix} = \begin{pmatrix} 1.8 \times 10^3 & 0 \\ 0 & 1.86 \times 10^3 \end{pmatrix}$$ Mass matrix

$$Cc := \begin{bmatrix} 2csusp & (csusp \cdot Lb - csusp \cdot Lf) \\ (csusp \cdot Lb - csusp \cdot Lf) & (csusp \cdot Lb^2 + csusp \cdot Lf^2) \end{bmatrix} = \begin{pmatrix} 5.091 \times 10^3 & -763.675 \\ -763.675 & 1.235 \times 10^4 \end{pmatrix}$$ Damping matrix

$$Kk := \begin{bmatrix} 2 \cdot ksusp & (ksusp \cdot Lb - ksusp \cdot Lf) \\ (ksusp \cdot Lb - ksusp \cdot Lf) & (ksusp \cdot Lb^2 + ksusp \cdot Lf^2) \end{bmatrix} = \begin{pmatrix} 8 \times 10^4 & -1.2 \times 10^4 \\ -1.2 \times 10^4 & 1.94 \times 10^5 \end{pmatrix}$$ Stiffness matrix

vel := 30.54 Normal speed for the vehicle

A bump in the road

$$Yroad(x) := \begin{cases} \frac{1}{4}\cdot\sin(x) & \text{if } 0 < x < \pi \\ 0 & \text{otherwise} \end{cases} \qquad x := 0, 0.001 .. 10$$

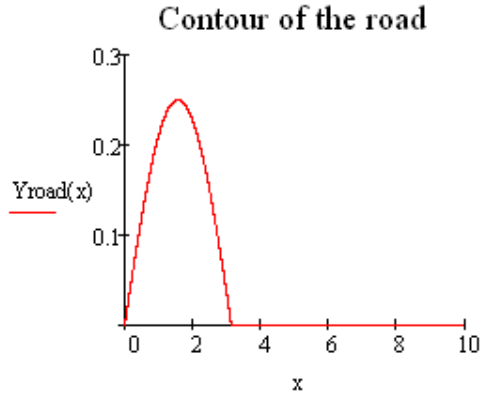

$$yroad(t) := \begin{cases} \frac{1}{4}\cdot\sin(vel\cdot t) & \text{if } 0 < t < \frac{\pi}{vel} \\ 0 & \text{otherwise} \end{cases} \qquad t := 0, 0.001 .. .2$$

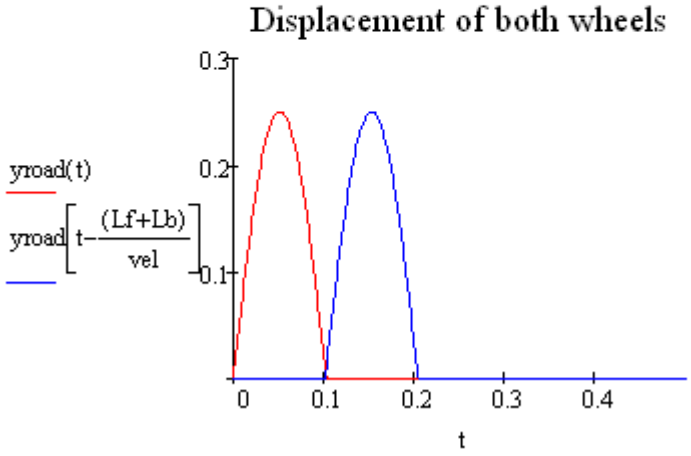

$$Ff(t) := csusp \cdot \left(\frac{d}{dt} yroad(t) \right) + ksusp \cdot yroad(t)$$ First wheel

$$Fb(t) := csusp \cdot \left(\frac{d}{dt} yroad\left(t - \frac{Lf + Lb}{vel} \right) \right) + ksusp \cdot yroad\left(t - \frac{Lf + Lb}{vel} \right)$$ Second wheel

$$Fforce(t) := \begin{pmatrix} Ff(t) + Fb(t) \\ -Ff(t) \cdot Lf + Fb(t) \cdot Lb \end{pmatrix}$$

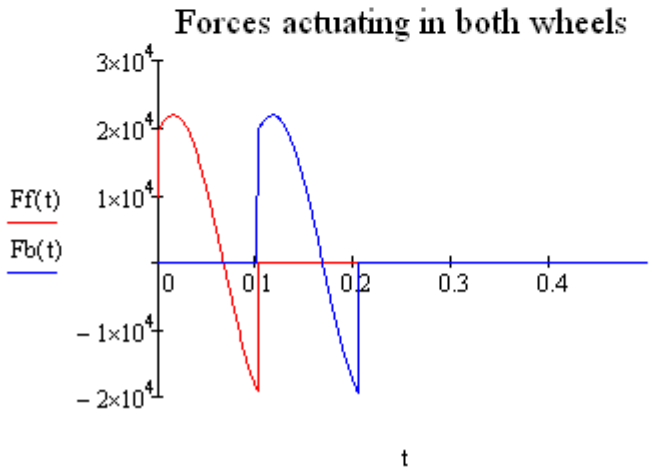

With the energy harvesting system:

$$Ffmax(t) := ctmax \cdot \left(\frac{d}{dt} yroad(t) \right) + ksusp \cdot yroad(t)$$ First wheel

$$Fbmax(t) := ctmax \cdot \left(\frac{d}{dt} yroad\left(t - \frac{Lf + Lb}{vel} \right) \right) + ksusp \cdot yroad\left(t - \frac{Lf + Lb}{vel} \right)$$ Second wheel

$$Ftmax(t) := \begin{pmatrix} Ffmax(t) + Fbmax(t) \\ -Ffmax(t) \cdot Lf + Fbmax(t) \cdot Lb \end{pmatrix}$$

We use the time integration (Runge-Kutta method) the movement of the chassis after passing through the bump.

From now on we assumed that the Lf = Lb:

$$ORIGIN := 1$$

$$to := 0$$

$$tmax := 5$$

$$Invalues := \begin{pmatrix} 0 \\ 0 \\ 0 \\ 0 \end{pmatrix}$$

$$D1(t,y) := \begin{bmatrix} y_3 \\ y_4 \\ \dfrac{Fforce(t)_1 - csusp \cdot y_3 - 2ksusp \cdot y_1}{Mvehicle} \\ \dfrac{Fforce(t)_2 - \left(csusp \cdot Lb^2 + csusp \cdot Lf^2\right) \cdot y_4 - \left(ksusp \cdot Lb^2 + ksusp \cdot Lf^2\right) \cdot y_2}{Jvehicle} \end{bmatrix}$$

$$S1 := rkfixed(Invalues, to, tmax, 1000, D1)$$

$$T1 := S1^{\langle 1 \rangle} \qquad Y'chassis := S1^{\langle 4 \rangle}$$

$$Ychassis := S1^{\langle 2 \rangle} \qquad \theta'chassis := S1^{\langle 5 \rangle}$$

$$\theta chassis := S1^{\langle 3 \rangle}$$

With the energy harvesting system:

$$D2(t,y) := \begin{bmatrix} y_3 \\ y_4 \\ \dfrac{Ftmax(t)_1 - ctmax \cdot y_3 - 2ksusp \cdot y_1}{Mvehicle} \\ \dfrac{Ftmax(t)_2 - \left(ctmax \cdot Lb^2 + ctmax \cdot Lf^2\right) \cdot y_4 - \left(ksusp \cdot Lb^2 + ksusp \cdot Lf^2\right) \cdot y_2}{Jvehicle} \end{bmatrix}$$

$$S2 := rkfixed(Invalues, to, tmax, 1000, D2)$$

$$T1 := S2^{\langle 1 \rangle} \qquad Y'cmax := S2^{\langle 4 \rangle}$$

$$Ycmax := S2^{\langle 2 \rangle} \qquad \theta'cmax := S2^{\langle 5 \rangle}$$

$$\theta cmax := S2^{\langle 3 \rangle}$$

$t := 0, 1 .. 1000$

Accelerations of the chassis:

$$ddYYchassis(t) := \frac{Fforce\left(T1_t\right)_1 - csusp \cdot Y'chassis_t - 2ksusp \cdot Ychassis_t}{Mvehicle}$$

$$ddYYcmax(t) := \frac{Ftmax\left(T1_t\right)_1 - ctmax \cdot Y'chassis_t - 2ksusp \cdot Ychassis_t}{Mvehicle}$$

The amount of energy we could harvest with the energy harvesting system is:

$$Power(t) := Fforce\left(T1_t\right)_1 \cdot Y'chassis_t$$

$$Pmax(t) := Ftmax\left(T1_t\right)_1 \cdot Y'cmax_t$$

$A2(t) := Pmax(t) - Power(t)$ Amount of energy harvest with the system